NANO-PETROPHYSICS OF AVALON SHALE OF THE DELAWARE BASIN OF WEST TEXAS & SOUTHEASTERN NEW MEXICO, USA

By

ARINZE COLLINS ADON

Presented to the Faculty of the Graduate School of

The University of Texas at Arlington in Partial Fulfillment of the Requirements

For the Degree of

MASTER OF SCIENCE IN GEOLOGY

THE UNIVERISITY OF TEXAS AT ARLINGTON

May 2019

Abstract

NANO-PETROPHYSIS OF AVALON SHALE OF THE DELAWARE BASIN OF WEST TEXAS & SOUTHEASTERN NEW MEXICO, USA

Arinze Collins Adon, MS

The University of Texas at Arlington, 2018

Supervising Professor: Qinhong (Max) Hu

The Avalon Shale is a Permian-aged stratum and represents a significant rock unit within the Bone Spring, of the Delaware basin of West Texas and Southeastern New Mexico. The Delaware Basin has witnessed increased drilling activities owing to the resurgence in the Permian basin, where organic-rich shales of the Wolfcamp, Avalon and tight Bone Spring Sands, are the primary targets. However, this boom in production has been constrained by low recovery from tight reservoirs. This problem has continued to attract attention because of the need to improve the reservoir performance of the Bone Spring wells.

To achieve this objective, a suite of experiments has successfully been performed on several samples from the Avalon Shale, and the First and Second Bone Spring Sands. Results indicate that the Avalon Shale has a moderate hydrocarbon generating potential, with sample AS 1AF-6342 having an S2 value of 4.76 mgHC/g, TOC value of 2.25%, T_{max} value of 438^{o}C, is oil prone and rich in type II/III kerogen (marine and terrestrial origin). Average TOC content across the Avalon shale is 1.1%, and 1% for the Second Bone Spring Sand. XRD results indicate the existence of five different lithofacies within the Avalon Shale and two among the Bone Spring Sands. The average porosity ranges from 0.2 to 6.7% for Avalon Shale, 4.9 to 8.1% for the First Bone Spring Sand, and 0.3 to 3% for the Second Bone Spring Sand. Absolute permeability is very low and relative permeability will be affected by the co-presence of oil and gas within the Avalon Shale. MICP results show that organic, intragranular,

intergranular and microfracture pores, are common pore types found within the Avalon Shale, whereas inter-clay platelets, organic pores, intragranular, intergranular and microfractures are found in the Second Bone Spring Sand. Spontaneous imbibition results show that the Avalon Shale is moderately water-wet, intermediary water wet for First Bone Spring Sand and oil-wet for the Second Bone Spring Sand. Pore structure characteristics show that clay composition, compaction and the ratio of intragranular pores to microfractures greater than 1 μm, all affects porosity. The higher the microfracture-sized pores greater than 1 μm, the lower the porosity. in summary, targeting the source rock at 6342 feet for horizontal drilling will be ideal, as it has the optimal mineralogy to maintain a good fracture growth. Furthermore, the overlying rocks at 6328-6331 feet are porous, rich in quartz and will support a good fracture height.

Acknowledgements

I would like to thank Annabelle Lopez of the New Mexico Bureau of Geology, for providing access to the Bureau's extensive core library and geologic data. Without her help, this research wouldn't have been possible. I would like to thank DrillingInfo for donating DrillingInfo subscription to Dr. Hu's research group.

A special thanks goes to my advisor Dr. Qinhong Hu for his guidance during this process, and my committee members, Dr. John Wickham and Dr. Mortaza Pirouz for their time and support. I also acknowledge the contributions of Golam Kibria, Qiming Wang and Zeynep Doner, who are members of the research group, for their guidance and assistance during this process.

Finally, I would like to thank my brothers; Ikemefuna K. Adon and Ugochukwu M. Adon, for their unwavering support and love throughout these years.

December 21, 2018

Table of Contents

Abstract……ii

Acknowledgements……..v

Table of Contents…….…...vi

List of Illustrations…….viii

List of Tables……... x

Chapter 1 Introduction……...11

Chapter 2 Geologic Setting……...…….14

Chapter 3 Methods……..……17

3-1 Sample Procurement……..……...…17

3-2 X-ray Diffraction (XRD) Analysis ……24

3-3 Pyrolysis and TOC…….…….25

3-4 Vacuum Saturation……..…….25

3-5 Mercury Intrusion Capillary Pressure (MICP)……...….26

3-6 Density Measurements ……...…29

3-7 Spontaneous Imbibition…….……32

Chapter 4 Results……...…35

4-1 X-ray Diffraction (XRD) Analysis…….…….35

4-2 TOC and Pyrolysis…….….42

4-3 Vacuum Saturation…….……51

4-4 Core Porosity and Permeability…….....……52

4-5 Mercury Intrusion Capillary Pressure (MICP)…….…….....53

4-6 Density Measurements …….....……57

4-7 Spontaneous Imbibition……..…….……58

4-8 Production Data……...…….….....62

Chapter 5 Discussion…….....64

5-1 Production Potential.....64

5-2 Porosity and Permeability..... 66

Chapter 6 Conclusion and Recommendation…….…...71

Appendix A…….....72

Appendix B……79

References…… 83

List of Illustrations

Figure 1-1 Avalon Shale location in the Delaware basin of W. Texas & S/E New Mexico….....12

Figure 2-1 Evolution of the Delaware basin between late Pennsylvania and Permian ….....…15

Figure 2-2 Stratigraphic column of the Bone Spring formation …….....16

Figure 3-1 3 well locations in the Permian basin …….....….17

Figure 3-2 Photos of samples taken upon arrival at UTA…….....20

Figure 3-3 Set up for vacuum saturation experiment…….…….....……26

Figure 3-4 Micrometrics Autopore IV 9520……..…….……28

Figure 3-5 Apparatus for Archimedes displacement …….....31

Figure 3-6 Stoppered bottle for pycnometry test…….....……32

Figure 3-7 Setup for spontaneous imbibition..... 34

Figure 4-1 Pie chart displaying the mineralogy for each samples…….....……37

Figure 4-2 Bar chart displaying each sample's quartz, carbonate and clay composition….....40

Figure 4-3 Lithofacies classification scheme for Avalon shale and Bone Spring Sands.....41

Figure 4-4 Source potential logs for Avalon Shale.....44

Figure 4-5 HC indicator and maturity logs for Avalon Shale.....45

Figure 4-6 Pseudo Van Krevelen Plot for Avalon Shale.....46

Figure 4-7 Kerogen quality plot for Avalon Shale.....47

Figure 4-8 Source potential logs for Second Bone Spring Sand.....48

Figure 4-9 HC indicator and maturity logs for Second Bone Spring Sand.....49

Figure 4-10 Pseudo Van Krevelen Plot for Second Bone Spring Sand.....50

Figure 4-11 Pore throat size distribution for Avalon Shale and Second Bone Spring Sand.....56

Figure 4-12 Volume of pore throat diameter from Avalon Shale and Second Bone Spring Sand.....56

Figure 4-13 DI water and DT2 imbibition slope for Avalon Shale.....60

Figure 4-14 DI water and DT2 imbibition slope for Second Bone Spring sample.....60

Figure 5-1 Amoco Federal 11 well log …….....65

Figure 5-2 XRD result for sample AS 1AF-6342.....66

Figure 5-3 Pore size distribution of samples against clay composition.....67

Figure 5-4 Leco TOC plotted against sample.....68

Figure 5-5 Pore size distribution against sample maturity.....68

Figure 5-6 MICP porosity against clay composition.....69

Figure 5-7 Pore size distribution against carbonate composition.....70

List of Tables

Table 3-1 Core sample information and well location…….....19

Table 3-2 Sieve fractions and sample size designation…….20

Table 3-3 Properties of standard saturating and immersion fluids …….....24

Table 4-1 XRD results for individual minerals…….....35

Table 4-2 Lithofacies description for each samples…….....41

Table 4-3 TOC and Pyrolysis result for Avalon Shale and Second Bone Spring Sand.....42

Table 4-4 Edge accessible porosity results from vacuum saturation.....51

Table 4-5 Helium porosity and permeability results for Avalon Shale.....52

Table 4-6 First Bone Spring Sand porosity and permeability result from Saga Pet. Corp.....53

Table 4-7 Summary of MICP results.....54

Table 4-8 Apparent bulk density results from liquid displacement and pycnometry.....57

Table 4-9 Imbibition slopes for DI water and DT2.....61

Table 4-10 Production data for the 3 wells.....63

Chapter 1

Introduction

The shale revolution has transformed the U.S. natural gas industry which has been on a decline since the early 1980's (EIA, 2014). This boom has helped reduce the United States reliance on imported energy and making it a net exporter of natural gas for the first time since 1957 (EIA, 2018). Current preliminary estimates show that the United States has outpaced Saudi Arabia and Russia to become the largest crude oil producer, with an average production of about 10.7 million b/d in 2018 and is projected to rise to 11.5 million b/d in 2019 (EIA, 2018). According to the report of EIA (2018) , the rise in production since 2005 has been attributed to unconventional shale oil, in which the Permian basin is a major player. The Permian basin market outlook for 2023 stands at 5.4 million barrels of oil, which is twice the basin's output of 2017 (IHS Markit, 2018). However, the play development has been constrained by the problem of low recovery (Hughes, 2014). This problem has been attributed to limited hydrocarbon (oil and gas) diffusion from the rock matrix to the fracture network (Hu and Ewing, 2014).

The Delaware and Midland basins (Figure 1-1) are the two most productive sub-Permian basins, with the Delaware deeper and thicker but still less developed with fewer wells (Bevers, 2017). The Delaware basin is asymmetrical, dipping sharply from the central platform on the eastern side, and a shallow structural dip on the western flank. In the Delaware portion of the Permian basin, the Avalon Shale is the primary focus of this research. The Avalon Shale is a stratigraphic interval within the upper First Bone Spring carbonate member and this carbonate interval sits on top of three sequences of Bone Spring sands (first, second and third sands), that are interbedded with carbonate sequences. Extensive multiple pay zones, in the Avalon Shale, First, Second and Third Bone Spring Sands, make the Bone Spring formation the ideal candidate for this study.

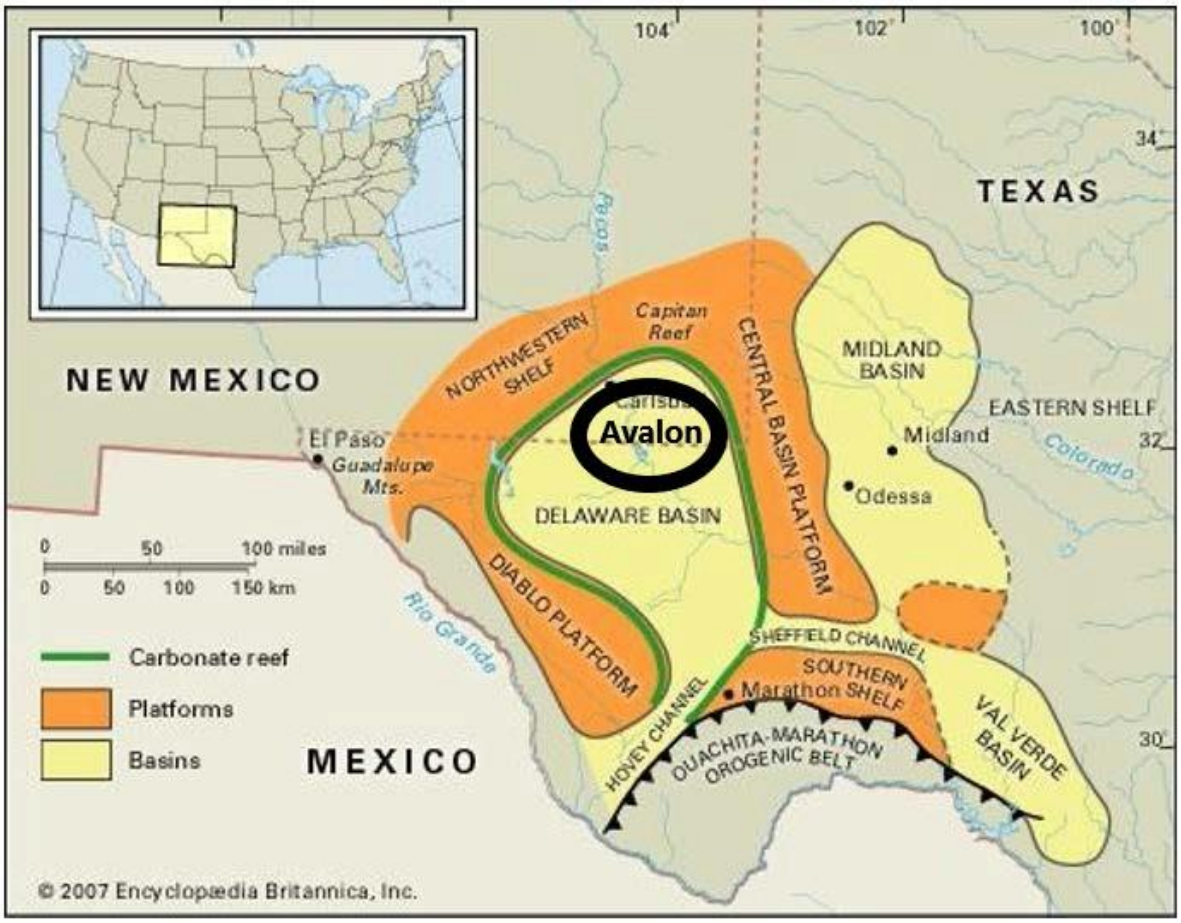

Figure 1-1: Avalon Shale location in the Delaware basin of West Texas & Southeastern New Mexico (modified from Encyclopedia Britannica, 2007)

Avalon Shale has a porosity range between 8% to 15% and permeability from 0.5 to 7.2 md (Broadhead et al., 2004). For the Bone Spring Sands, porosity averages 4% (Jarvie, 2008), and 2.0 md for permeability (Montgomery, 1997). For horizontal wells, the oil decline rate of Bone Spring Formation stands at roughly 91% for 3-year period and that is the highest decline rate for any known shale play (Hughes, 2014). According to Hughes (2014), a recent growth within the play has been attributed to new technologies that involve extensive capital and infrastructural input in order to compensate for the short fall from the basin's steep production decline. Therefore, to help improve the understanding of the Bone Spring reservoir properties related to production decline, different experimental approaches will be performed.

Production potential of the Avalon Shale and Bone Spring Sands will be evaluated using TOC/pyrolysis and XRD analysis to help identify sweet spots and optimal landing zones. Spontaneous imbibition with DI water will determine the rock-fluid characteristics of the selected samples. To characterize the pore structure, the mercury injection capillary pressure (MICP) test will provide useful information on bulk density, porosity, pore volume, total pore area, pore throat size distribution, median pore throat size, while permeability and tortuosity can be estimated. Vacuum saturation, pycnometry-Archimedes displacement, and core porosity and permeability techniques will provide data on bulk density, porosity and permeability. This research aims to highlight and demonstrate the relationship between the derived measurements, and to show how important they are in improving the reservoir performance of the Bone Spring formation.

Chapter 2

Geologic Setting

The Delaware basin is bounded by captian reef and shelf areas in the north, southern shelf in the south, diablo platform to the west and the central basin platform in the east. Development and sedimentation of the Delaware basin (Figure 2-1) began in the late Paleozoic after the ancient Tobosa basin was deformed by the Ouachita-Marathon fold belt in the Hercynian orogeny. The advancing Ouachita-Marathon fold belt coincided with the uplift of the central basin platform, leading to the development of the Delaware and Midland basins (Cys and Gibson, 1988). Kinley et al. (2008) noted that about 20,000 ft. of lower Pennsylvanian through Permian sediments were deposited in the basin, as well as several marked structural changes (Adams 1965). Clastic sedimentation continued until the middle Pennsylvanian, followed by carbonate deposits due to increased tectonic activities from middle to late Pennsylvanian (Hills, 1984). By the beginning of the Permian, tectonism has peaked (Hills, 1985), before a rotational tilting towards the east by the late Permian. Hills (1985) reported reduced tectonic activity at this stage. The Triassic period had red beds accumulation, while there is no record of Jurassic to early cretaceous sediments, suggesting the existence of a subaerial erosion (Hills, 1984). Hills and Galley (1988) noted that apart from the western edge, the sandstones and shelf limestone deposited during the middle cretaceous sea transgressions were unaffected by the late tectonic activities including Laramide orogeny. Structural trends in the western margin of the Delaware basin experienced renewed igneous activity in the Tertiary, resulting in maturation of source rocks n localized areas (Baker and Pawlewicz, 1987). Shepard and Walper (1982) reported that extensional faulting and over printing of basin style to be the final deformation stage in this basin.

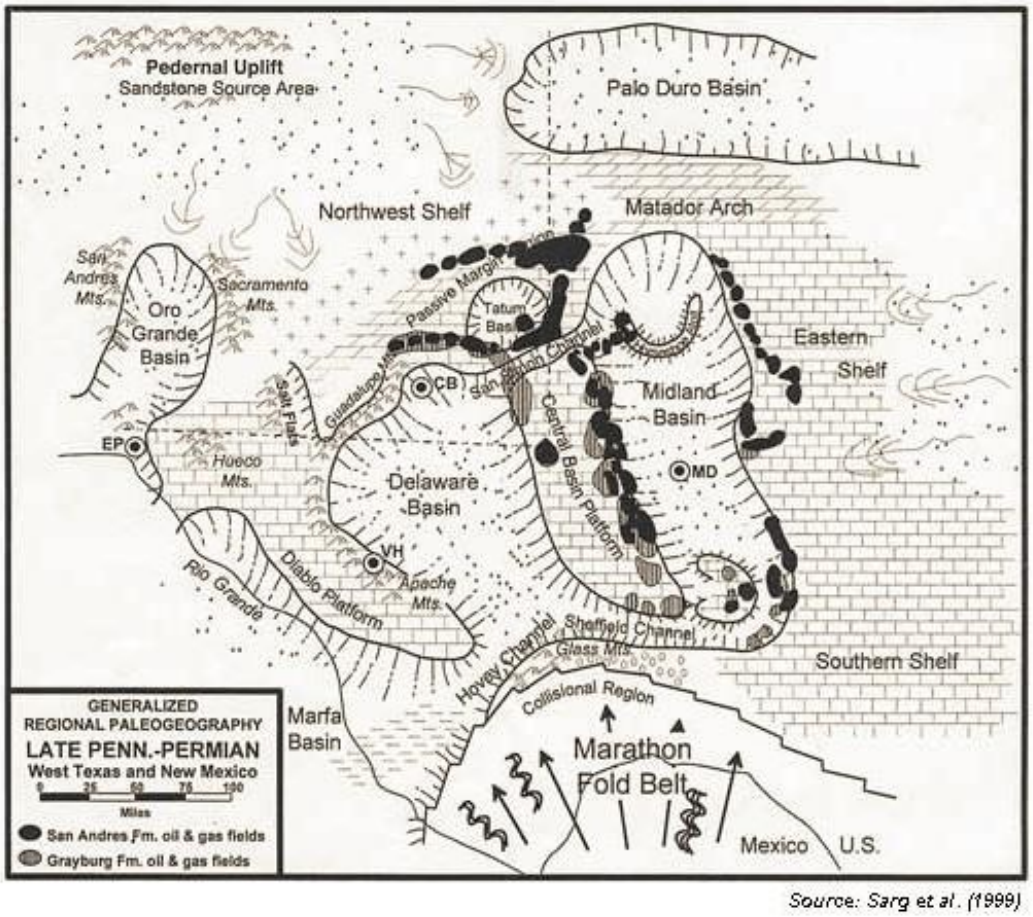

Figure 2-1: Map showing evolution of the Delaware basin between late Pennsylvania and Permian (Sarg et al., 1999)

Stratigraphically, the Permian deposits varies from clastic to evaporites in the basin and carbonates to red beds and evaporites in the shelves. Avalon Shale of the Delaware basin is of Leonardian age and lies within the first Bone Spring carbonate member (Figure 2-2). The Avalon Shale is characterized as an alternating succession of organic mudstones and deep-water carbonates deposited as the sea level fell (Rittenhouse et al., 2017). Worrall et al. (2011) noted that there is no apparent stratigraphic distinction between the Upper and Lower Avalon, but the Upper Avalon is the most targeted because it is shaly and the gamma ray log often shows over 100 units, while the lower Avalon is silty with gamma ray values less than 80 units. The organic-rich mudstones of the upper and lower

Avalon are considered to be high quality potential reservoir, whereas the middle Avalon with high percentage of carbonate is not. Avalon Shale can amass up to 600 ft. of potential reservoir from a 950 ft. formation (Worrall et al., 2011). It has been exploited by conventional wells, but the advances in horizontal drilling, combined with multiple stage fracturing, has drawn increased attention to explore its potential as unconventional reservoirs. Since 2008, over 400 wells targeting the Avalon have been drilled (Nester et al., 2014). The reservoir is predominantly gas filled at the western edge of the basin and transitions to light oil and condensate towards the east end (Nester et al., 2014).

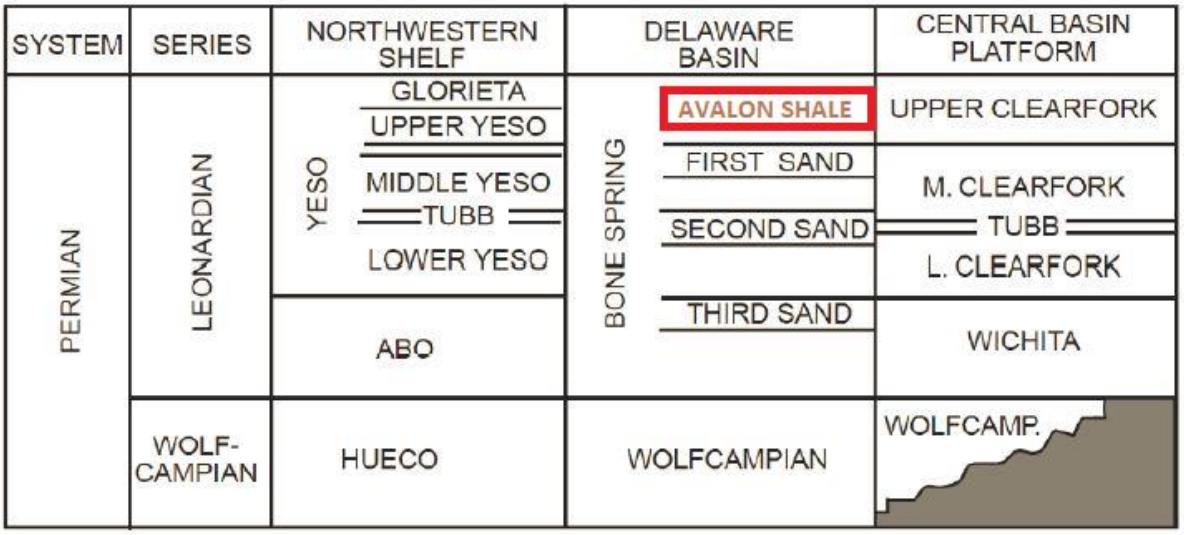

Figure 2-2: Stratigraphic column of the Bone Spring formation, showing the location of Avalon Shale, First and Second Bone Spring Sands. Not shown are carbonate sequences bounding the Avalon, First, Second and Third Bone Spring Sands (modified from Montgomery, 1997)

Chapter 3

Methods

3–1 Sample Procurement

Rock samples for this research include whole core and slabs obtained from the core repository at the New Mexico Bureau of Geology. Cores were taken from two vertical wells in Eddy County and one from Lea County in New Mexico. Figure 3-1 below displays the well location for Amoco Federal 11 #001 (Well 1), Potts Federal #003 (Well 2) and State FU #005 (Well 3). Well 1 is approximately 20.5 miles from well 2 and 41.4 miles from well 3, while wells 2 and 3 are approximately 43.2 miles apart. Their geolocations are shown in Table 3-1. For easier sample identification, core samples from Amoco Federal 11 #001 are represented with AS-1AF, Potts Federal #003 with BS1 3PF, and the State FU #005 with BS2 5SFU: 'AS' represents Avalon Shale, 'BS1' for First Bone Spring Sand, and 'BS2' for the Second Bone Spring Sand.

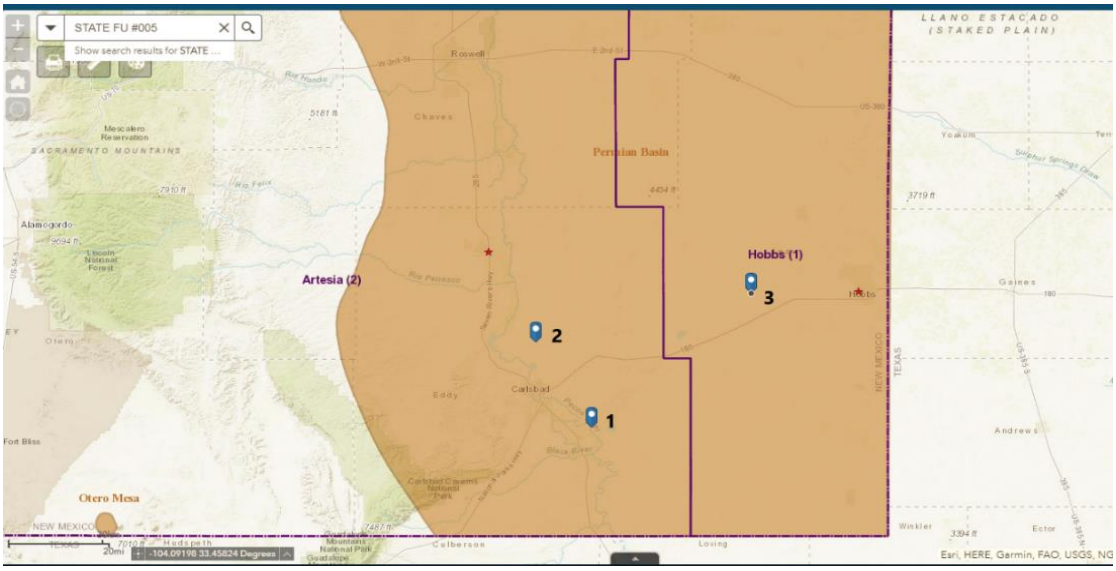

Figure 3-1: 3 well locations in the Permian basin. Well 1 represents cores for Avalon Shale, well 2 & well 3 for First and Second Bone Spring sands respectively (New Mexico Oil Conservation division).

Table 3-1 below contains well location, unique sample identification number, and weight of core samples when they arrived. Sample identification number is derived from the well name and the sample depth, and is assigned the moment the samples arrived at the UTA lab. The workflow detailed below entails all activities performed from the initial (sample processing) and final stages (laboratory experiments). It is important to note that before any experiment was conducted, the sample is oven dried for 2 days at 60^{o}C to remove moisture, and then placed in a desiccator of 10% humidity and allowed to cool for at least 30 minutes.

A complete work flow is provided as follows:

- Core samples are assigned unique identification numbers
- Air-dry weights are taken, dimensions measured, any lamination noted
- Photo documentation with a camera and a microscope (Figure 3-2)
- Sample cutting and size reduction (to 12 cylindrical plugs, cubes, half cubes, thin slabs, sieve sized fractions from GRI+ down to powder) (Table 3-2)
- XRD analysis is performed at the UTA Shimadzu Center using the powder fractions
- Pyrolysis and TOC experiment are done at GeoMark Research Laboratory
- Archimedes displacement tests are performed (for cubes X, Y, and Z)
- Vacuum saturation tests for cubes and the plugs using deionized water
- Core plug porosity and permeability tests
- MICP tests for cube X
- Pycnometry tests (performed on the GRI+, GRI and Size C samples with a deionized water and DT2 solution – a solution of n-decane and toluene in the volumetric ratio of 2:1)
- Spontaneous imbibition test with deionized water for cube samples.

Table 3-1

Core sample information and well location

Well No	Well Name	County	Geo-location	Formation	Depth (ft.)	Sample ID	Weight (g)	Additional Info
1	Amoco Federal 11 #001	Eddy	Lat. 32.3182526/Long -104.052475 NAD83	Avalon Shale	6298 6299-6300 6328-6331 6342 6384	AS 1AF-6298 AS 1AF-(6299-6300) AS 1AF-(6328-6331) AS 1AF-6342 AS 1AF-6384	1637.7 163.59 253.61 1384.7 457.23	Active oil well Spud: 08/04/1979; first oil/gas produced: 08/08/2002
2	Potts Federal #003	Eddy	Lat. 32.5698357/Long -104.2410278 NAD83	First Bone Spring Sand	6147 6257	BS1 3PF-6147 BS1 3PF-6257	206.4 244.14	Active gas well Spud: 03/01/2003
3	State FU #005	Lea	Lat. 32.713707/Long -103.5197983 NAD83	Second Bone Spring Sand	10224 10243 10252	BS2 5SFU-10224 BS2 5SFU-10243 BS2 5SFU-10252	375.72 157.42 153.5	Plugged & Abandoned: 10/27/1993

Table 3.2

Sieve fractions and sample size designation

Size designation	Mesh	Size fraction (diameter)	Equivalence (µm)
Plug		2.54 cm	30735
Cube		1.0 cm	9086
GRI+	#8 to #12	1.70 - 2.36 mm	2030
Size A	#12 to #20	841 – 1700 µm	1271
GRI	#20 to #35	500 – 841 µm	671
Size B	#35 to #80	177 – 500 µm	339
Size C	#80 to #200	75 – 177 µm	126
Powder	<#200	<75 µm	<75

a.

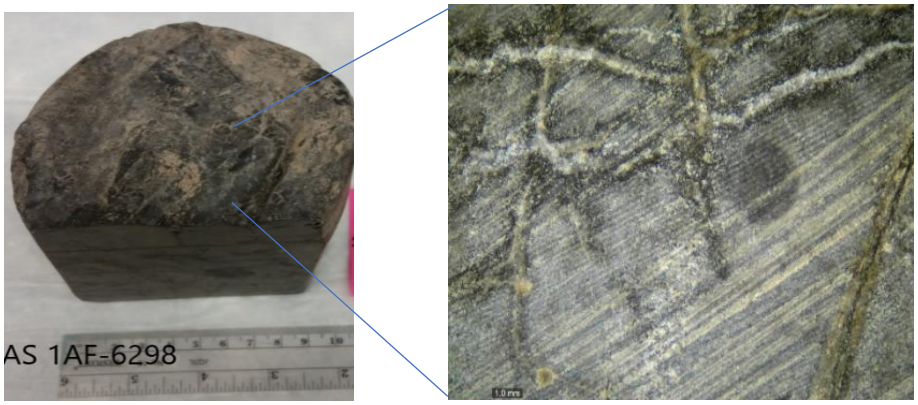

b.

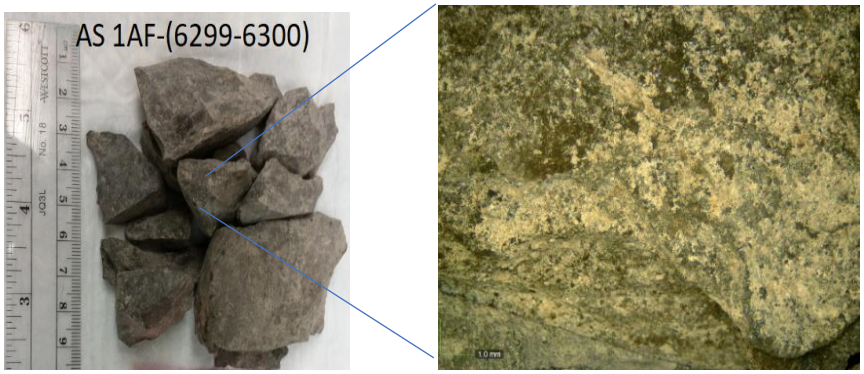

c.

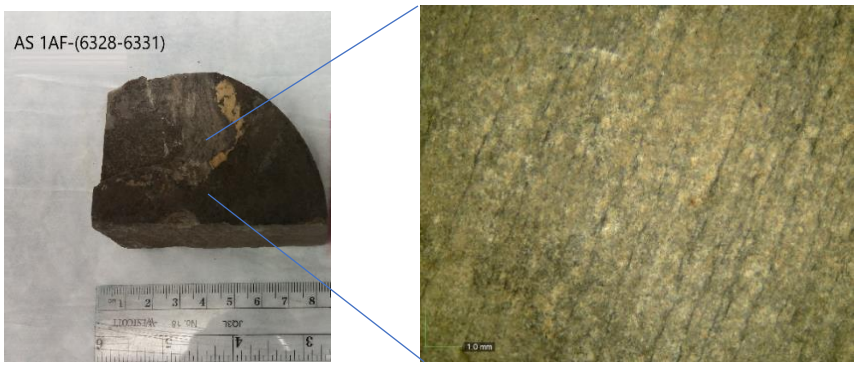

d.

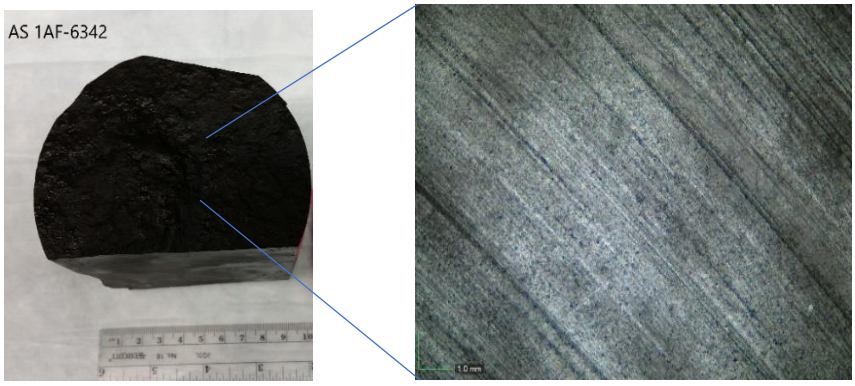

e. 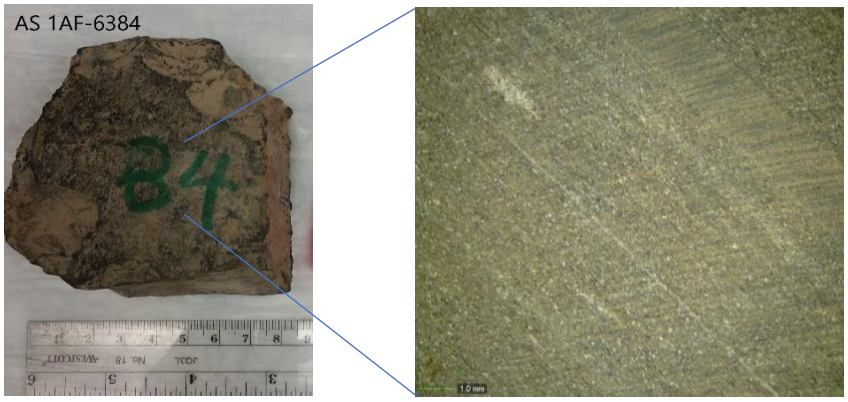

f. 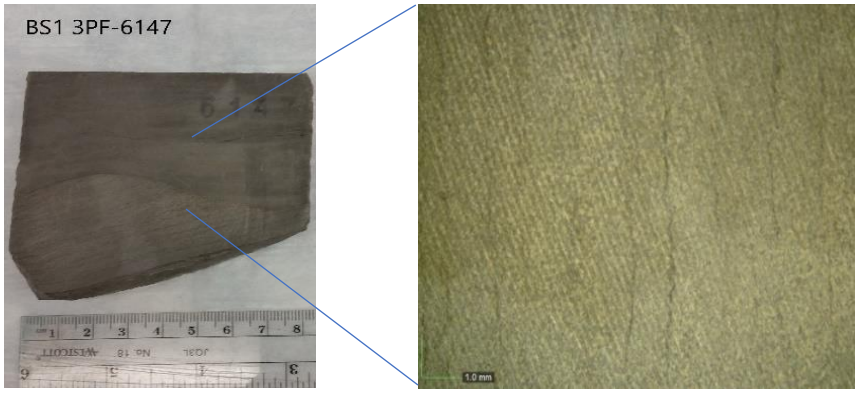

g. 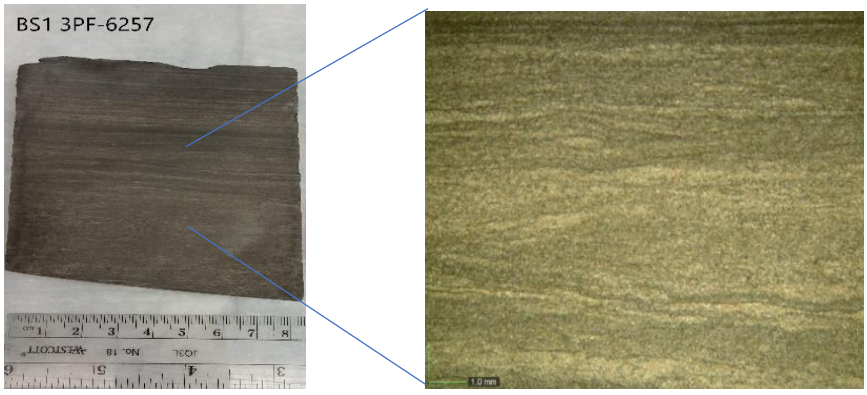

h. 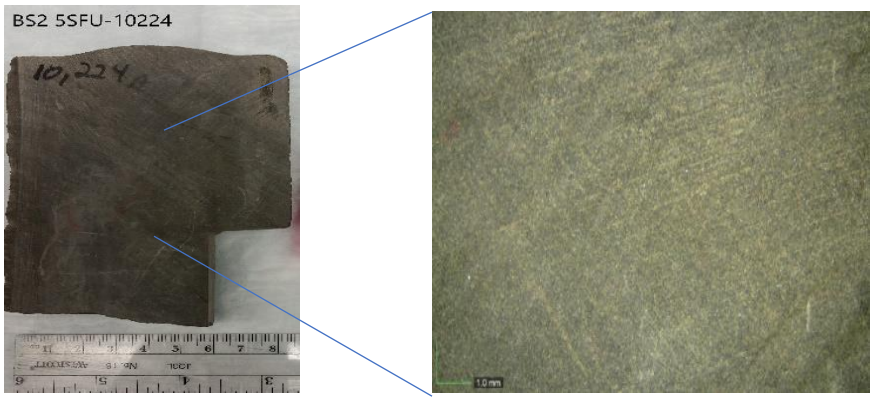

i. 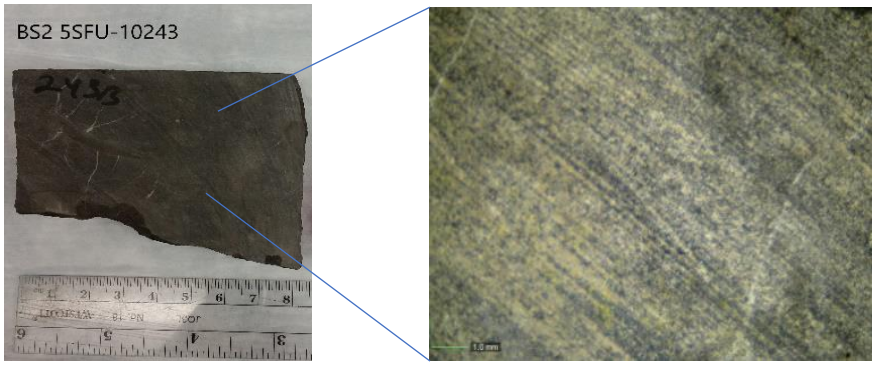

j. 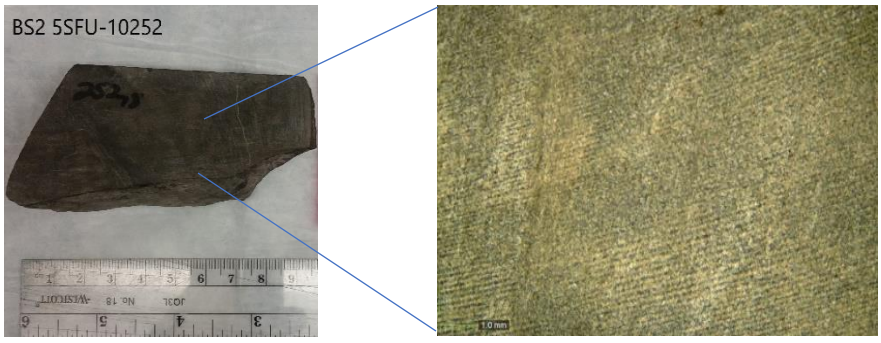

Figure 3-2: Photos of samples taken upon arrival at UTA. Unique sample identification number is displayed on images

3-1-1 Immersion and Saturating Fluids

For the purpose of this research, deionized water (DI water) and DT2 mixture (a solution of n-decane and toluene in the ratio of 2:1) were used as saturating and immersion fluids, as analogs for hydrophilic and hydrophobic fluids. This is in accordance with core analysis technique (API 40), and previous works by Alexander et al. (1981), Howard (1991), and Washburn et al. (1922). Table 3-3 compares the standard immersion and saturating fluids under four important parameters.

Table 3-3

Properties of standard saturating and immersion fluids (modified from Kuila et al., 2013)

Liquid	Surface tension (dyne s/cm)	Dynamic viscosity (centipoise)	Penetration coefficient (cm/s)	Vapor pressure (mmHg)
Acetylene tetrachloride	31.1	1.610	965.6	72.37
DI water	72.7	1.002	3630.9	17.55
Kerosene	27.5	1.233	1115.2	2.21
n-Hexane	18.5	0.312	2964.7	121.41
Octane	21.6	0.541	1998.1	10.43
Decane	23.8	0.912	1305.5	0.96
Isopar V	27.0	18.005	75.0	<0.08

3-2 X-ray Diffraction (XRD) Analysis

The XRD analysis was performed by the team at UTA Shimadzu Center, and the detailed steps can be found in Appendix A. Powder size fractions from the earlier workflows is compacted in the XRD sample holder before calibration, then processed before opening the peak profile spectrum. The minerals are then identified, before generating a model for the minerals. At the end, a pattern deconvolution is carried out before the data are saved. The generated data were then used in generating a ternary plot for sCore lithofacies identification.

3-3 Pyrolysis and TOC (total organic carbon)

Pyrolysis and TOC experiments were performed at GeoMark Research, and the detailed steps can be found in Appendix B. Derived data include carbonate percentage, S1 (which is a measure of the free hydrocarbons before they undergo pyrolysis), S2 (quantity of hydrocarbons generated during thermal pyrolysis), S3 (carbon dioxide produced during the breakdown of kerogen), T_{max} (temperature at the maximum hydrocarbon generation and it equals the temperature at the peak of S2), vitrinite reflectance (calculated value obtained from T_{max}), HI (hydrogen index), OI (Oxygen Index), normal oil content, and PI (production index).

3-4 Vacuum Saturation

Vacuum saturation is a technique for measuring the edge-only accessible porosity distribution of a sample material, and the apparatus is shown in Figure 3-3. The setup is made up of a sample chamber that is connected to a fluid reservoir, CO_2 cylinder and a vacuum pump. DI water is the saturating fluid for this experiment because of its higher penetration coefficient (Table 3-3). Test samples were first oven dried for 48 hours at 60^{o}C and cooled in a desiccator of 10% relative humidity for at least 30 minutes. The new weight of the sample is taken before putting in the sample chamber. First evacuation is done till pressure is less than 0.1 torr (timeframe is minimum of 8 hours and can be sustained for 12 to 18 hours for overnight samples). After the first evacuation, CO_2 is injected for 30 minutes at 50 psi, before another round of evacuation (that lasts at least eight hours) to about 0.1 torr. Next, de-ionized water is injected from the reservoir into the chamber, before pressurizing the submerge samples with CO_2 for three to four hours. This pressurization further drives the fluid into the evacuated pore spaces before the saturated samples are weighed immediately as the experiment concludes. After the first weighing, the sample is re-submerged in the saturating fluid, excess fluid is blotted off with a moistened kimwipe before re-weighing the second time, to reduce error.

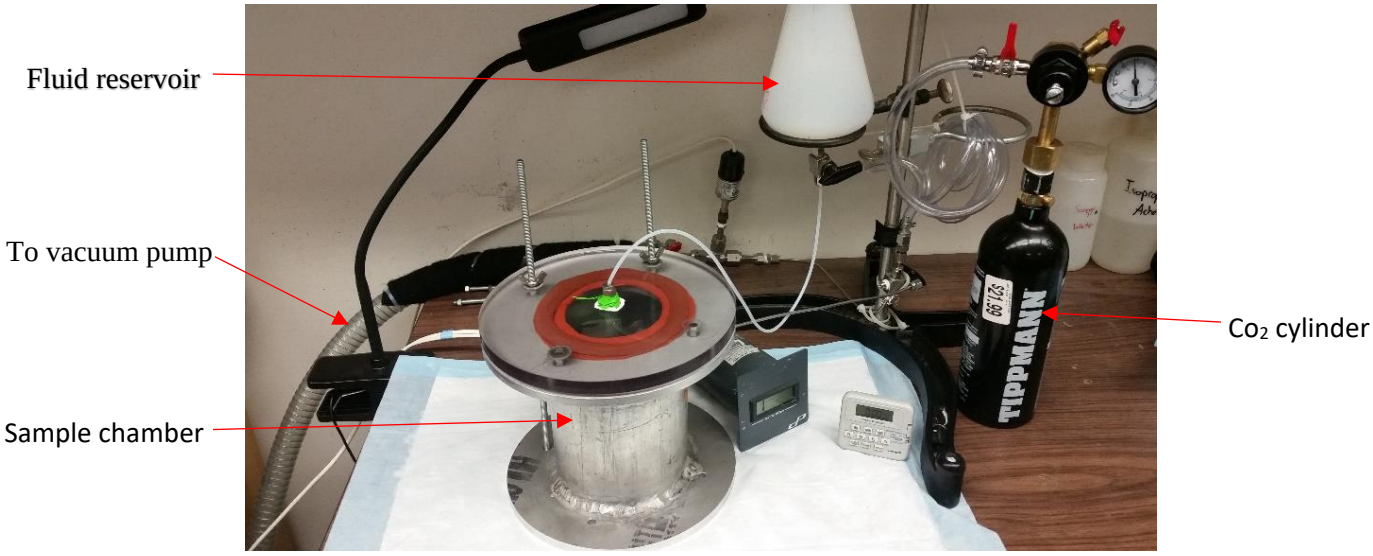

Figure 3-3: Setup for vacuum saturation experiment

3-5 Mercury Injection Capillary Pressure (MICP)

The experimental procedure involves applying incremental pressures to a sample immersed in a non-wetting fluid like mercury. Pressure and the corresponding volume increase are then recorded, before calculating the pore size distribution with a Washburn equation (Equation 3-4; 1921). According to Washburn (1921), the pressure needed to invade the pore is inversely proportional to pore size. Information on bulk density, porosity, pore volume, total pore area, pore throat size distribution and the median pore throat size can be obtained directly from the test, while permeability (Katz and Thompson, 1986) and tortuosity (Hager, 1998) can be derived indirectly from the result.

$$\Delta P = -\frac{2\gamma \cos\theta}{R} \qquad \text{……..……..} \quad (3\text{-}4)$$

Where,

- ΔP = External pressure applied (psia)
- Y = Surface tension for mercury (dynes/cm)
- θ = Contact angle between mercury and pore wall (degrees)
- R = Pore throat radius (μm)

A Micrometrics Autopore IV 9520 (Figure 3-4) is the laboratory equipment for conducting this test. A cube-sized sample is first oven dried at 60-degree for 48 hours, before it is placed in a desiccator of 10 percent humidity for at least 30 minutes. The new sample weight is recorded, before the sample is put in a penetrometer after the right conditions (like maximum measurable pore volume and bulb volume) have been set. To help expel moisture and air from the vacuum, a low-pressure of 99.993% vacuum is achieved. Mercury is then allowed to flow in at 30 psi, before the sample is moved to a high-pressure chamber, where the pressures will be increased incrementally. Each pressure step has an equilibration time of about 10 secs, and the pressure can reach up to 60,000 psi before mercury extrusion begins. Once the analysis is done, both the sample and penetrometer are taken out of the machine and weighed before the residual mercury is removed from the sample. The pore throat diameter can then be calculated using the modified Washburn (1921) equation, as reported by Wang et al. (2016).

$$\Delta P = -\frac{2\gamma_{Hg}(R)\cos\theta_{Hg}(R)}{R} \quad \text{..... (3-5)}$$

Figure 3-4: Micrometrics Autopore IV 9520

Katz-Thompson (1987) equation for calculating permeability is shown below.

$$k = \left(\frac{1}{89}\right)(L_{max})^2 \left(\frac{L_{max}}{L_c}\right) \phi S(L_{max}) \quad \text{..... (3-6)}$$

Where,

- k = absolute permeability (μm^2)
- L_{max} = pore throat diameter at maximum hydraulic conductivity
- L_c = pore throat diameter taken at threshold pressure
- Φ = porosity of the sample (in %)
- $S(L_{max})$ = mercury saturation at L_{max}

Hagger (1998) equation for calculating tortuosity is shown below.

$$\tau = \sqrt{\frac{\rho}{24k\,(1+\rho V_{tot})} \int_{\eta=r_{c,min}}^{\eta=r_{c,max}} \eta^2 f_v(\eta)\, d\eta} \qquad \text{..... (3-7)}$$

Where,

- ρ = density
- V_{tot} = total pore volume
- τ = tortuosity
- $\int_{n=rc,min}^{n=rc,max} \eta 2\ fv\ (\eta)\ d\eta$ = pore volume distribution

3-6 Density Measurements

The bulk density has a direct relationship with porosity, and the apparent bulk densities for Avalon Shale and the Bone Spring samples were determined using the Archimedes displacement and pycnometry methods.

The Archimedes displacement method consists of a wire basket, which is hung by an external support and submerged in a beaker (not touching the beaker, Figure 3-5) containing deionized water, and placed on top of a balance. The reading of the balance is adjusted to zero before weighing the sample. A processed (W_1, oven dried and cooled with a desiccator) cube sample is then immersed completely in the wire basket (in the beaker containing deionized water). The sample weight equals the mass of water displaced and is recorded as 'W_s'. The sample is then oven dried for 48 hours at 60^{o}C and re-weighed again for a new oven-dried weight 'W_2'. Equation 3-8 below was used in calculating the apparent bulk density.

$$\text{Apparent bulk density} = \frac{\text{Average oven dry weight}}{\frac{\text{Ws}}{\text{fluid density}}} \quad \text{..... (3-8)}$$

Where,

- Average oven dry weight = $(W_1 + W_2) / 2$
- Fluid density = 0.9980 g/cm^3 (DI water)

The pycnometry test for the Gas Research Institute recommended mesh sizes (GRI+ and GRI) and Size C sample size, were conducted with a 10ml and 5ml stoppered bottles called pycnometers (Figure 3-6). Deionized water and DT2 solution (a solution of n-decane and toluene in the ratio of 2:1) are the two saturating fluids used for this test. Prior to starting this test, the various size fractions were oven dried at 60^{o}C for 48 hours, and then cooled in a desiccator for 30 minutes at 10% relative humidity. For large samples, 2 g of each sample (W_1) was carefully poured into a clean dry pycnometer to avoid spilling. The pycnometer plus the oven-dried sample is then weighed on an analytical balance as W_2. Fluid is carefully added to fill up the pycnometer, ensuring that adhering sample inside the bottle is washed back into the container. The stopper is then added to seal it, ensuring that no trap air is retained in the bottle, while excess fluid is expelled through the capillary tube of the pycnometer. The pycnometer is cleaned, before weighing the pycnometer with the contents inside (rock sample plus fluid) as W_3. Finally, the contents inside the pycnometer are removed, and the bottle washed thoroughly. The pycnometer is filled with the same fluid, sealed with the stopper and then cleaned to remove excess water. The weight of pycnometer and fluid only (W_4) is then measured. This process for each sample is repeated twice for each fluid (deionized water and DT2 solution) for better accuracy. Equation 3-9 below is then used for calculating the apparent bulk density (g/cm^3).

$$\text{Apparent bulk density} = \frac{\text{W1}}{\frac{\text{W4}-\text{W3}+\text{W1}}{\text{fluid density}}} \quad \text{..... (3-9)}$$

Where,

- Oven dry weight = W_1
- Weight of pycnometer + fluid = W_4
- Weight of pycnometer + oven dry sample + fluid = W_3
- Fluid density = 0.990 (DI water), 0.7757 (DT2)
- DT2 = solution of n-decane + toluene (in the ratio of 2:1)

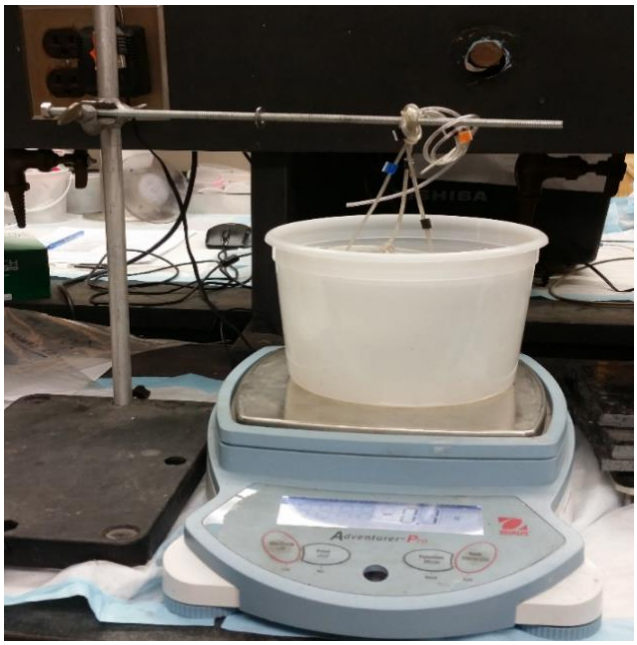

Figure 3-5: Apparatus for Archimedes displacement

Figure 3-6: Stoppered bottles for pycnometry experiment

3-8 Spontaneous Imbibition

Spontaneous imbibition studies the behavior of fluids when in contact with rocks. The slow process is driven by capillary forces (Ma, 1999), and is responsible for fracturing fluids invading the shale matrix (Roychaudhuri et al., 2011). Spontaneous imbibition is a critical characteristics for the recovery of oil, as it is the main source of fluid loss, capillary blockage or reduction in gas permeability, and may lead to formation damage (Bartoncello et al., 2014). Therefore, a better understanding will help in sustainable shale development.

The experimental setup in Figure 3-7 includes a high-precision weighing balance (with bottom weighing ability), a sample chamber and a computer for recording the weight change. Immersion fluid used for performing this test is DI water (deionized water). Rock sample size is a cube whose four side-walls have been epoxied (covered with thin coating to prevent fluid uptake). The sample dimensions (length, width and height) were first measured before epoxying, and then oved dried for 2 days at 60^{o}C. It is cooled in a desiccator at 10% relative humidity, weighed (60^{o}C oven dry weight), before other relevant properties are noted on the experiment datasheet. To limit evaporation from the petri dish, additional open containers with the same fluid (DI water) are placed in the imbibition chamber. The

sample is then lowered until it is in contact with the fluid on the petri dish, and the timer starts immediately to keep track of imbibition time as the new sample weight is tracked on the computer. A single run for each sample can last between 6 to 24 hours, before detaching the sample at the end of the experiment. To keep track of weight changes, the weight of sample with holder, weight of sample only, and the weight of petri dish are recorded quickly. A slightly moistened kimwipe is weighed and reweighed just after wiping residual fluids from the sample surface.

The imbibition slopes are derived with recognizance, that the square of imbibition time is proportional to the total volume of imbibed fluid when pore spaces are well connected (Yang et al., 2017; Equation 3-10)

$$V_{imb} = [(2P_c K_w \Phi S A_c^2/\mu_w)]^{0.5} \quad (3.9)$$

Where,

V_{imb} = total volume of the imbibed fluid

K_w = effective permeability of the media

μ_w = fluid viscosity

P_c = capillary pressure

A_c = cross-sectional area

Φ = porosity

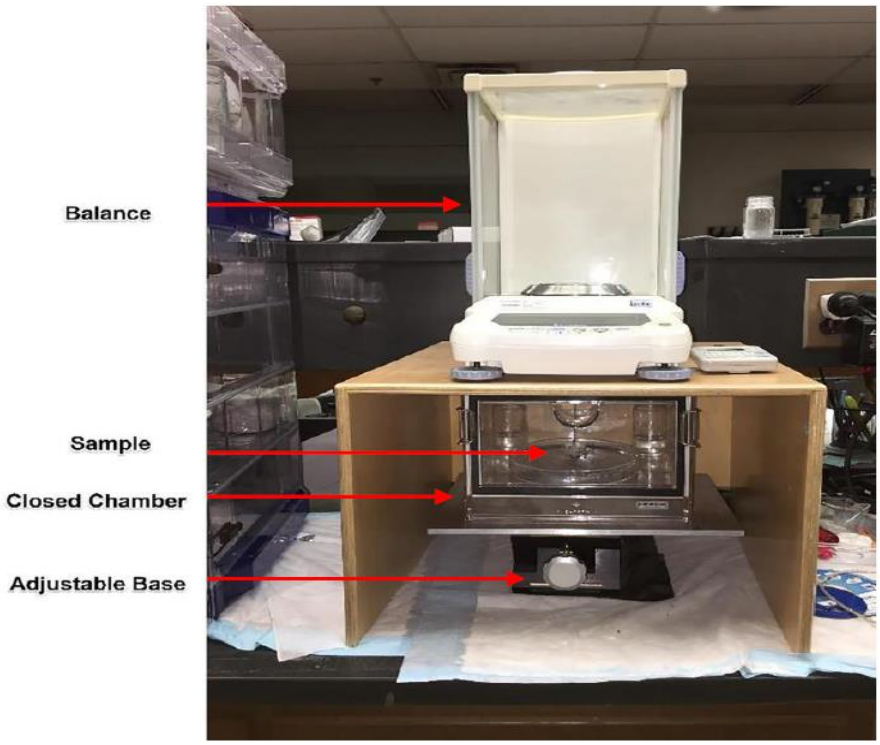

Figure 3-7: Setup for spontaneous imbibition

Chapter 4

Results

4-1 X-ray Diffraction

Table 4-1

XRD results showing weight (percentage) for individual minerals

Phase	Type	AS 1AF-6298	AS 1AF-(6299-6300)	AS 1AF-(6328-6331)	AS 1AF-6342	AS 1AF-6384	BS1 3PF-6257	BS2 5SFU-10224	BS2 5SFU-10252
Quartz	*Silica*	2.4	15.2	50.1	42.8	26.2	49.9	56.5	3.3
Cristobalite	*Silica*						1.4		
Albite	*Feldspar*		2.7	9	6.5	1.1	7.3	4.5	
Anorthite	*Feldspar*			22			15.9	16.7	
Orthoclase	*Feldspar*			0.9					
Pyrite	*Sulfide*		1	0.9	3.1	0.9	2.7	1.3	
Ulvospinel	*Oxide*				1.1		1.6	0.8	
Calcite	*Carbonate*	97.6	33.5	2.5	18	64.9			
High-Mg Calcite	*Carbonate*		31.9						
Ankerite	*Carbonate*		2.1	5.3	6	2.6	2.3		39.6
Dolomite	*Carbonate*							7.3	57.1
Illite	*Clay - Mica Group*		13.6	9.3	22.5	4.3	18.9	12.1	
Clinochlore	*Clay - Chlorite Group*							0.8	

XRD results in Table 4-1 indicate that 13 mineral phases exist within the Avalon and the Bone Spring Sands, with carbonates and silica groups the most predominant. This suggests that the samples are brittle enough to initiate a fracture (Berskin et al., 2001). Clay minerals like clinochlore and orthoclase feldspar are the least common mineral phases and are found at the depths of 6328-6331feet and 10224 feet in the Avalon and Second Bone Spring Sand, respectively. Dolomite is present in the second Bone Spring Sand, cristobalite in the first Bone Spring Sand, and High-Mg calcite was found only in the Avalon Shale. This variability in mineral composition suggests that the rocks will behave differently during hydraulic fracturing.

Pie charts of Figure 4-1 displays the mineral distribution for Avalon, First and Second Bone Spring samples. The highest percentage of clays within the Avalon Shale stands at 23% (at depth of 6342 ft. where the lithology is a mixed siliceous mudstone). This is consistent with Nester et al. (2014) who noted that Avalon Shale is a mixed carbonate-siliciclastic lithology rock, with commonly less than 25% clays. Equally, the silica occurrence is the highest at depths 6328-6331 ft. and 6342 feet for the Avalon Shale, 6257 feet for First Bone Spring Sand, and 10224 feet of the Second Bone Spring Sand. Rocks with high percentage of quartz tends to be brittle and hard, while mudrocks with high percentage of clays are less brittle. The knowledge of how brittle a rock is will help in predicting fracture height and growth patterns.

a.

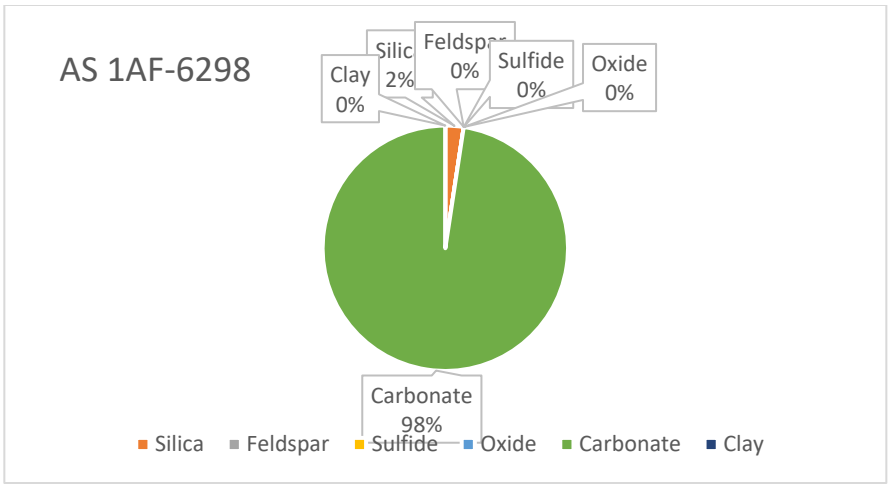
AS 1AF-6298
Clay 0%
Silic 2%
Feldspar 0%
Sulfide 0%
Oxide 0%
Carbonate 98%
Silica
Feldspar
Sulfide
Oxide
Carbonate
Clay

b.

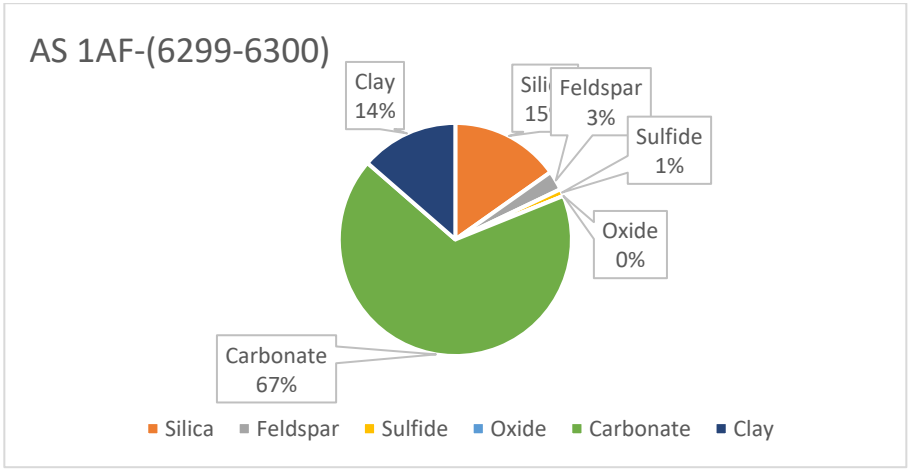
AS 1AF-(6299-6300)
Clay 14%
Sili 15
Feldspar 3%
Sulfide 1%
Oxide 0%
Carbonate 67%
Silica
Feldspar
Sulfide
Oxide
Carbonate
Clay

c.

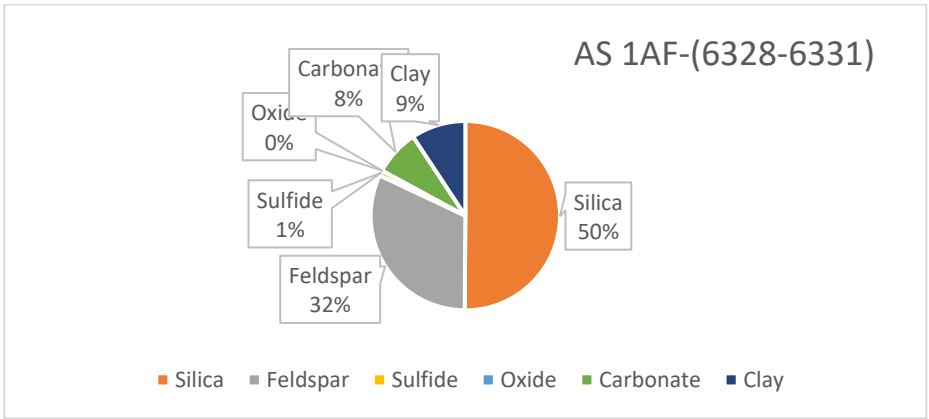
AS 1AF-(6328-6331)
Carbona 8%
Clay 9%
Oxide 0%
Sulfide 1%
Feldspar 32%
Silica 50%
Silica
Feldspar
Sulfide
Oxide
Carbonate
Clay

d.

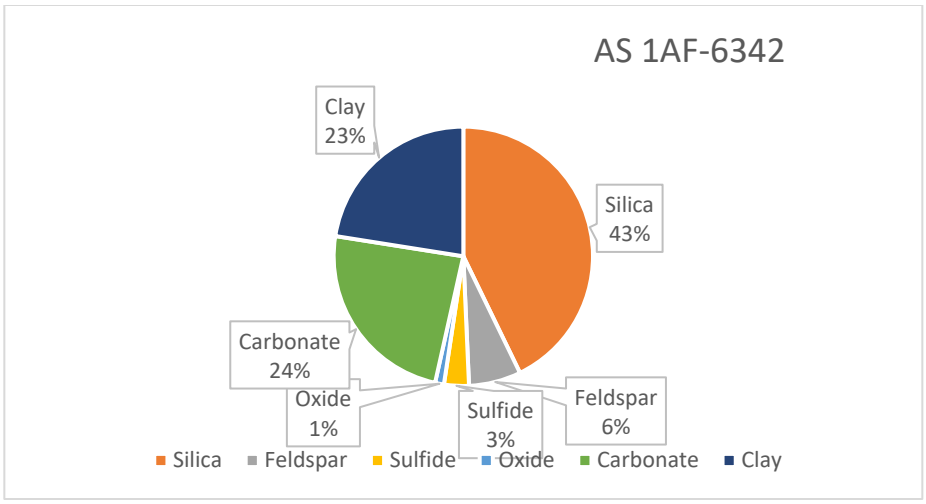
AS 1AF-6342
Clay 23%
Silica 43%
Carbonate 24%
Oxide 1%
Sulfide 3%
Feldspar 6%
Silica
Feldspar
Sulfide
Oxide
Carbonate
Clay

e.

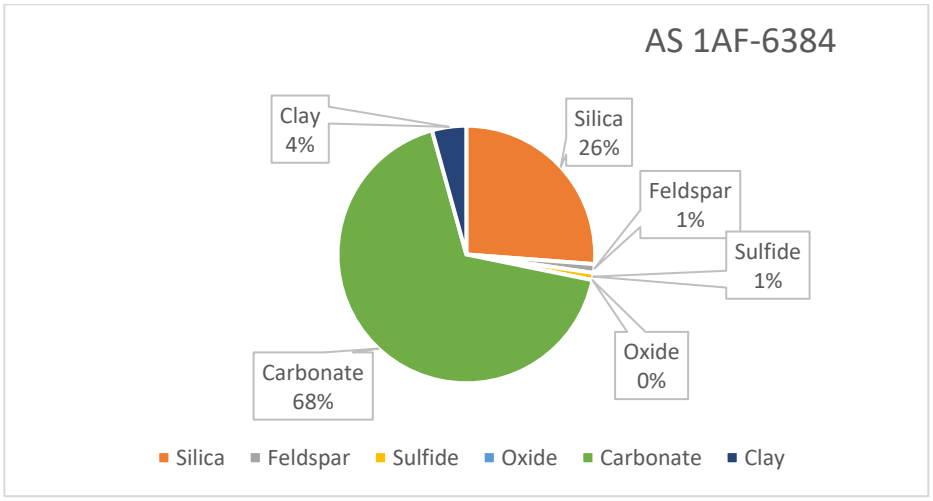
AS 1AF-6384
Clay 4%
Silica 26%
Feldspar 1%
Sulfide 1%
Oxide 0%
Carbonate 68%
Silica
Feldspar
Sulfide
Oxide
Carbonate
Clay

f.

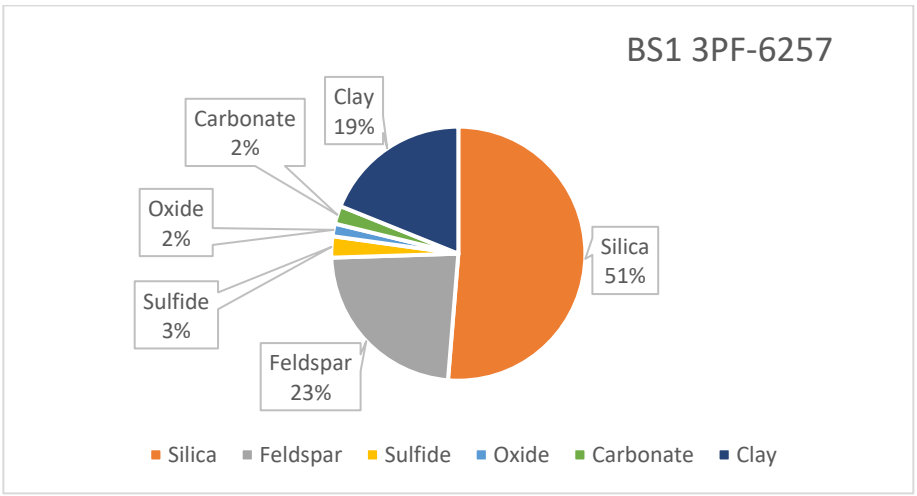
BS1 3PF-6257
Clay 19%
Carbonate 2%
Oxide 2%
Sulfide 3%
Feldspar 23%
Silica 51%
Silica
Feldspar
Sulfide
Oxide
Carbonate
Clay

g.

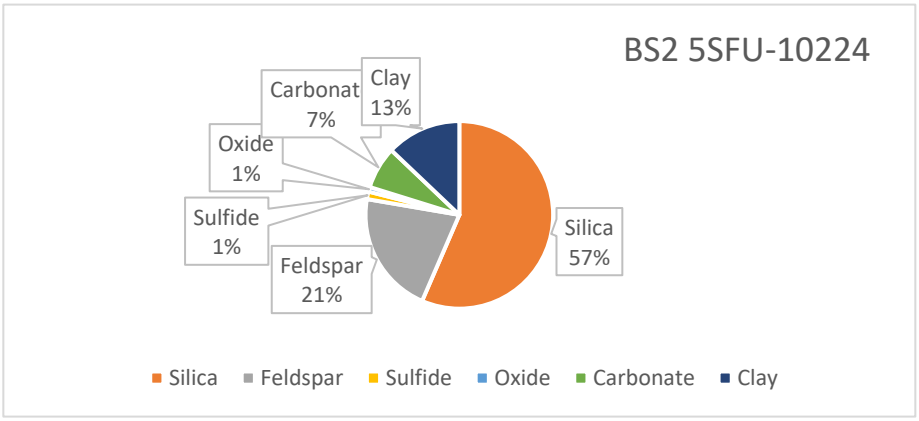

h.

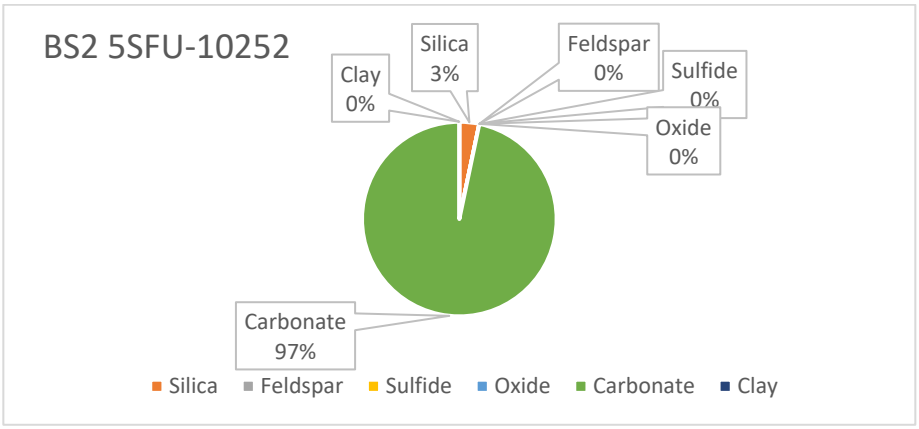

Figure 4-1: Pie chart showing the mineral composition for Avalon Shale, First and Second Bone Spring Sands

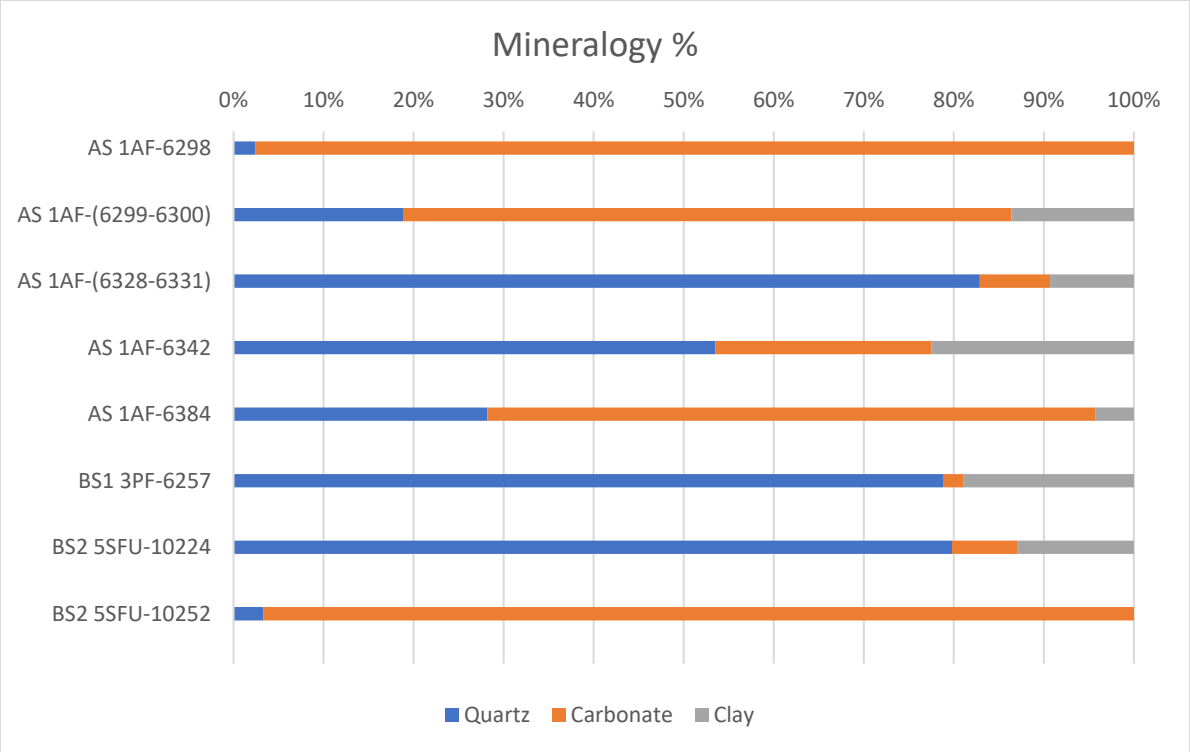

Figure 4-2: Bar chart showing each samples quartz, carbonate and clay composition

Figure 4-2 shows that quartz- and carbonate-rich sediments are the most common minerals within the Avalon and Bone Spring Sands, with a small percentage of clay. Clay is totally absent at the depth of 6298 ft. (Avalon Shale) and the Second Bone Spring Sand (depth of 10,252 feet), invariably where the lithotype is carbonate dominated. Figure 4-3 below is a ternary plot for Avalon Shale, First and Second Bone Spring Sands, while Table 4-2 is the lithofacies description of each sample. Five different lithofacies exist within the Avalon Shale, and two among the Bone Spring Sands.

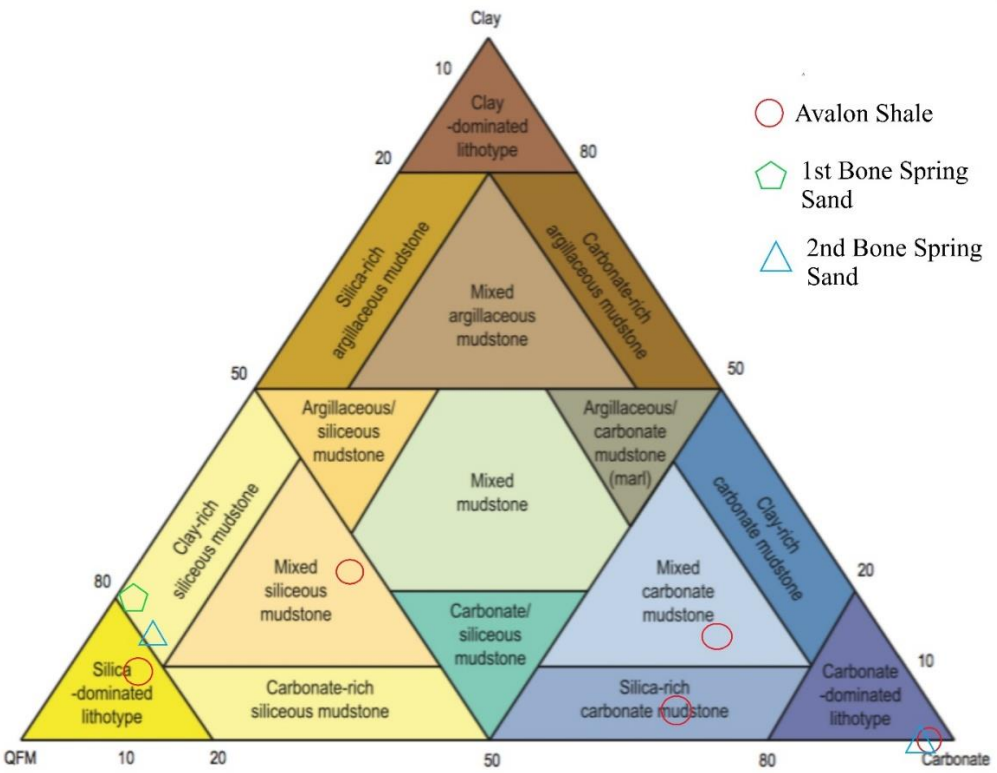

Figure 4-3: Lithofacies classification scheme for Avalon shale and Bone Spring Sands from the ternary diagram of Gamero-Diaz et al. (2013)

Table 4-2
Lithofacies description for each sample

Well No.	Formation	Depth (ft.)	Lithofacies description
1	Avalon Shale	6298	carbonate-dominated lithotype
		6299-6300	mixed carbonate mudstone
		6328-6331	silica-dominated lithotype
		6342	mixed siliceous mudstone
		6384	silica-rich carbonate mudstone
2	First Bone Spring Sand	6257	clay-rich siliceous mudstone
3	Second Bone Spring Sand	10224	clay-rich siliceous mudstone
		10252	carbonate-dominated lithotype

4-2 TOC and Pyrolysis

Table 4-3

TOC and pyrolysis results for Avalon Shale and Second Bone Spring Sand

Sample	AS 1AF-6298	AS 1AF-(6299-6300)	AS 1AF-(6328-6331)	AS 1AF-6342	AS 1AF-6384	BS2 5SFU-10224	BS2 5SFU-10252
Percent Carbonate (wt. %)	92.9	60.0	12.8	20.8	58.4	12.0	88.9
Leco TOC (wt. %)	0.44	1.47	0.21	2.25	1.00	1.04	0.90
Rock-Eval-2 S1 (mg HC/g)	0.08	1.05	0.11	0.96	0.62	0.66	0.58
Rock-Eval-2 S2 (mg HC/g)	0.45	2.76	0.25	4.76	1.64	1.41	1.50
Rock-Eval-2 S3 (mg CO2/g)	0.27	0.57	0.31	0.44	0.52	0.36	0.37
Rock-Eval-2 Tmax (°C)	439	440	440	438	442	440	443
Calculated %Ro (RE TMAX)	0.74	0.76	0.76	0.72	0.80	0.76	0.81
Hydrogen Index (S2x100/TOC)	102	188	119	212	165	136	166
Oxygen Index (S3x100/TOC)	61	39	148	20	52	35	41
S2/S3 Conc. (mg HC/mg CO2)	2	5	1	11	3	4	4
S1/TOC Norm. Oil Content	18	71	52	43	62	63	64
Production Index (S1/(S1+S2)	0.15	0.28	0.31	0.17	0.27	0.32	0.28

Pyrolysis and TOC (total organic carbon) results for Avalon Shale and the Second Bone Spring Sand are displayed in Table 4-3 above. TOC contents for Avalon Shale range between 0.21% (generally considered to be poor) to 2.25% (good quality TOC levels). TOC values of 2.2% is the average for shale source rocks while the value of 1.8% is the average for all source rocks (McDade et al., 1993). The elevated TOC levels of 2.25% at 6342 feet, suggests that sample AS 1AF-6342 is a potential source rock. Sample AS 1AF-(6328-6331) has the lowest TOC values, while samples AS 1AF-6298 and AS 1AF-(6328-6331) are considered organic-lean (TOC <0.5%). Despite the T_{max} values for Avalon Shale falls within the oil mature zone (T_{max} 435 – 450^{o}C), it will be early to jump into conclusion without consulting the S2 values (Figure 4-4). Peters (1986) noted that S2 values less than 0.2 is not reliable. S2 is an indication of the hydrocarbon generating potential. Therefore, sample AS 1AF-6342 and AS 1AF-(6299-6300) of the Avalon Shale with S2 values of 4.76 and 2.76, respectively, have a moderate potential to generate hydrocarbons. The calculated values of Vitrinite Reflectance (RETMAX) range from 0.72% (sample AS 1AF-6342) to 0.8% (AS 1AF-6384). The VR (%) is derived from equation 4-1 below and was used in calculating the maturity indicators (Figure 4-5). Pseudo Van Krevelen plot (Figure 4-6) and the kerogen quality plot (Figure 4-7) indicate generally a type II/III kerogen (oil or/and gas prone) for Avalon Shale.

$$RETMAX = (0.018 \times T_{max}) - 7.16 \quad \text{..... (4-1)}$$

Average TOC for Second Bone Spring samples (Figure 4-8) is 0.97%, which is less than the average values for all source rocks (TOC of 1.8%; McDade et al., 1993). T_{max} value for Second Bone Spring Sand falls within the oil or mature zone, but an S2 value less than 0.2 (Figure 4-8) makes the samples less reliable as a potential source rock. The maturity indicator for the Second Bone Spring Sand (Figure 4-9) indicate these samples to be within the oil generation window, while the Pseudo Van

Krevelen plot (Figure 4-10) indicate a type II kerogen and marine origin for the second Bone Spring samples.

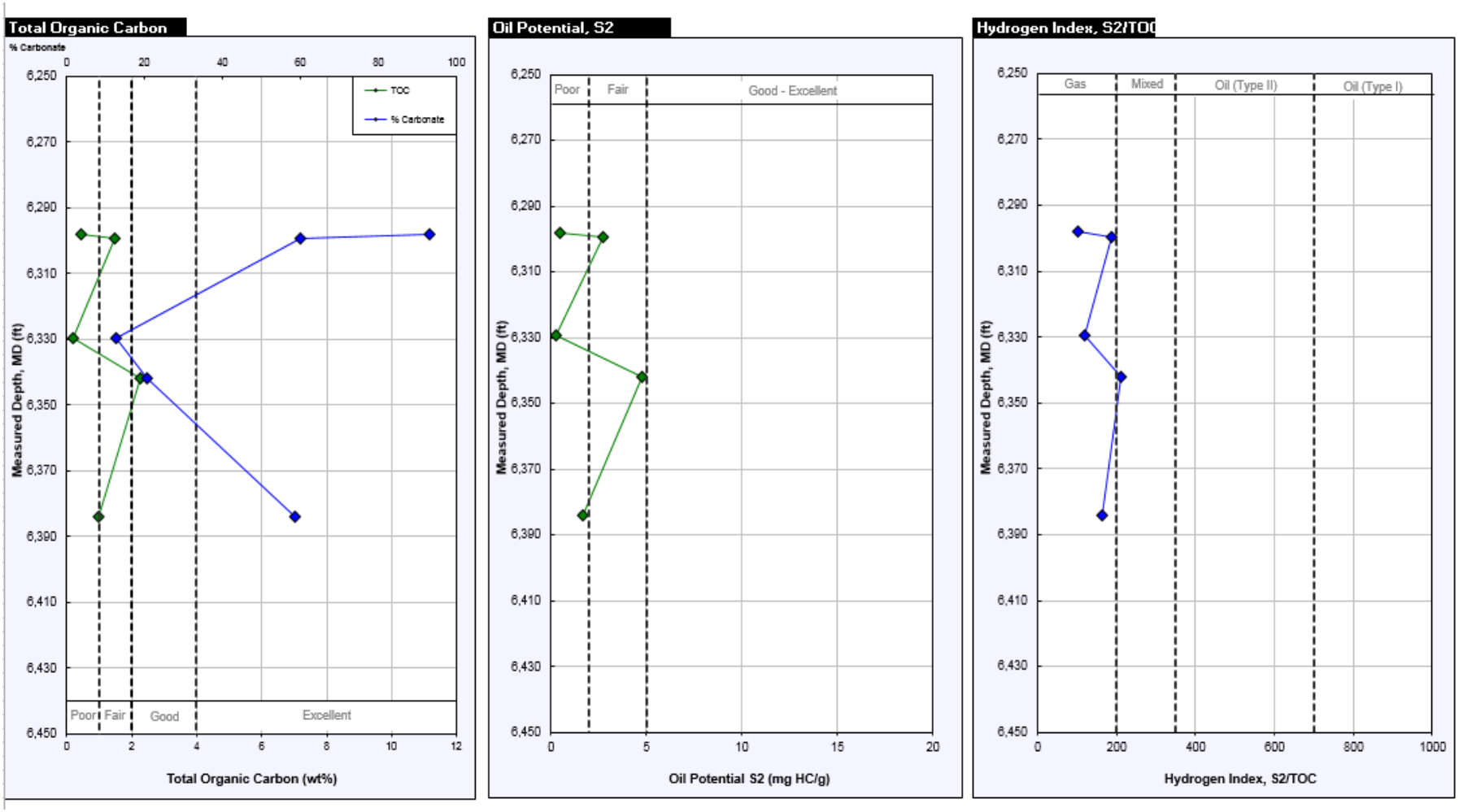

Figure 4-4: Source potential logs for Avalon Shale

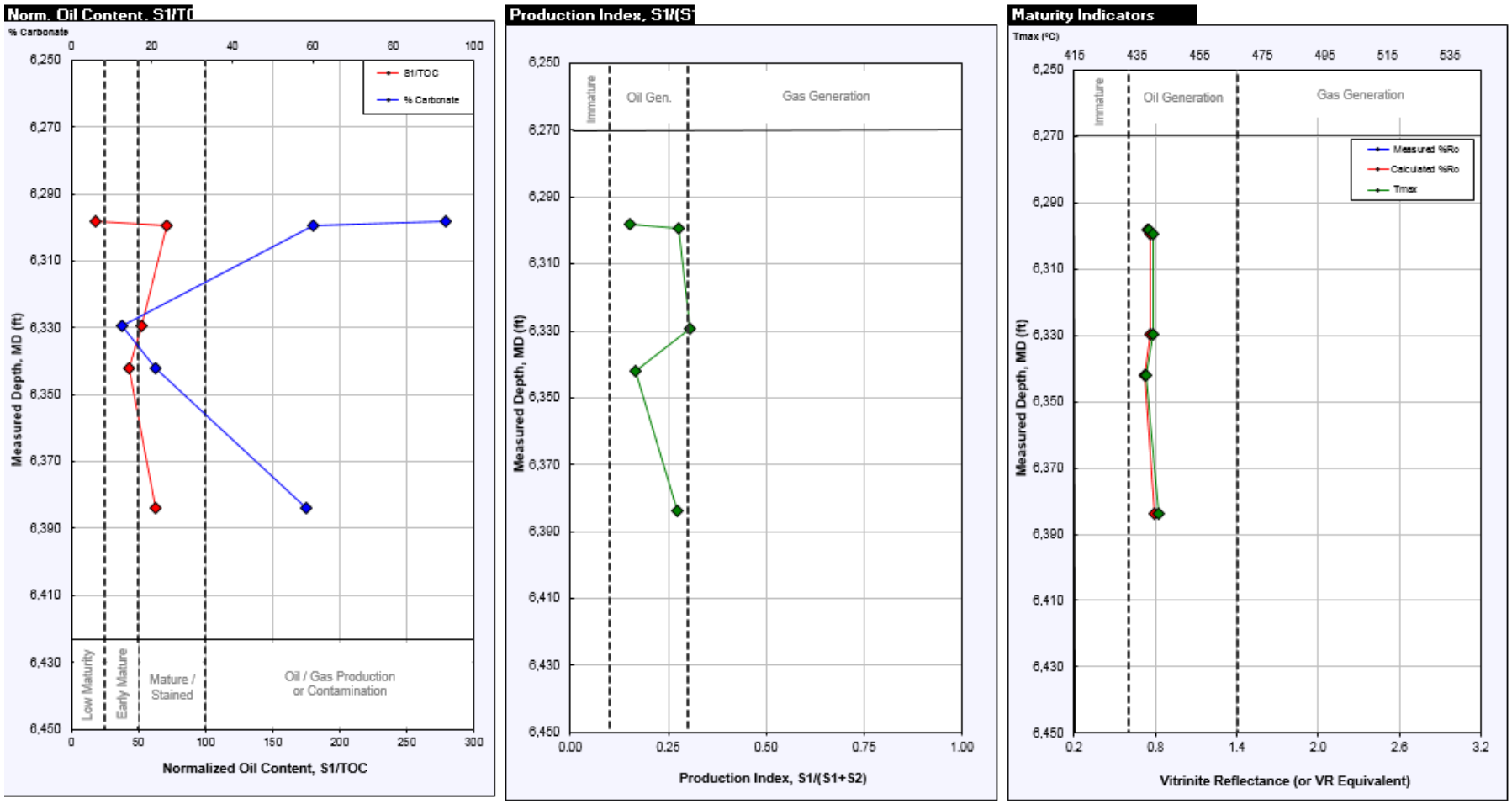

Figure 4-5: HC indicator and maturity logs for Avalon Shale

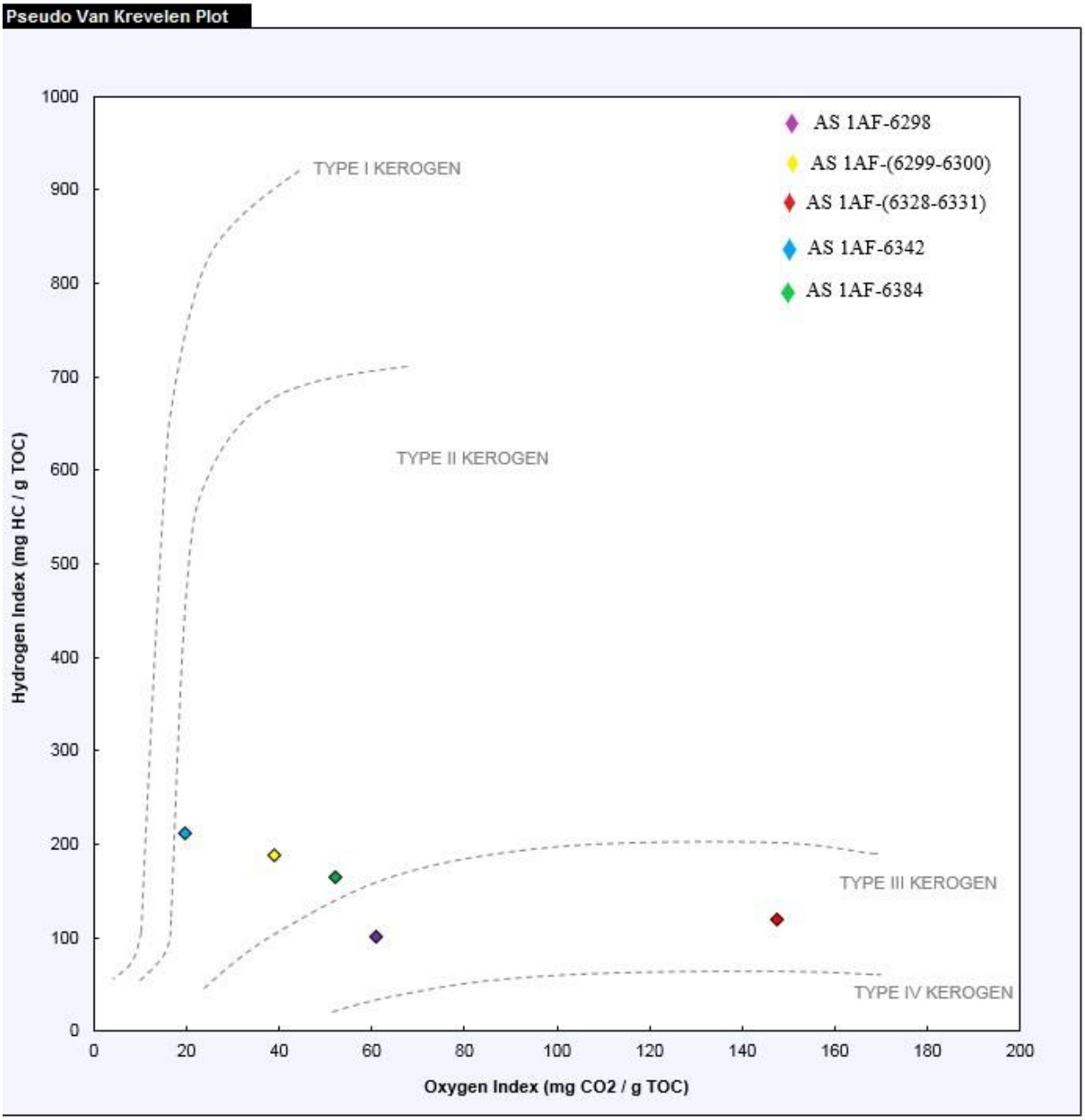

Figure 4-6: Pseudo Van Krevelen Plot for Avalon Shale

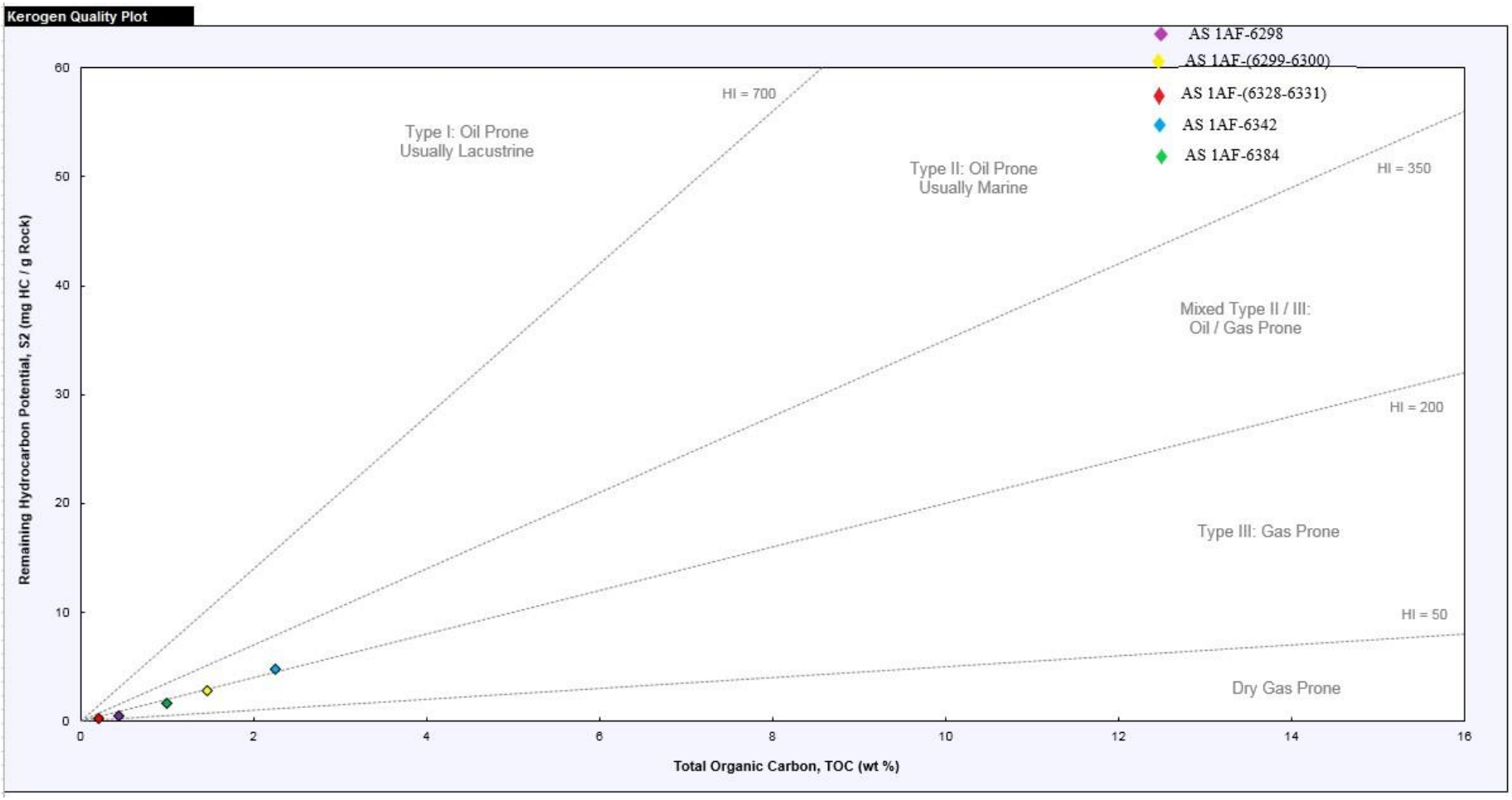

Figure 4-7: Kerogen quality plot for Avalon Shale

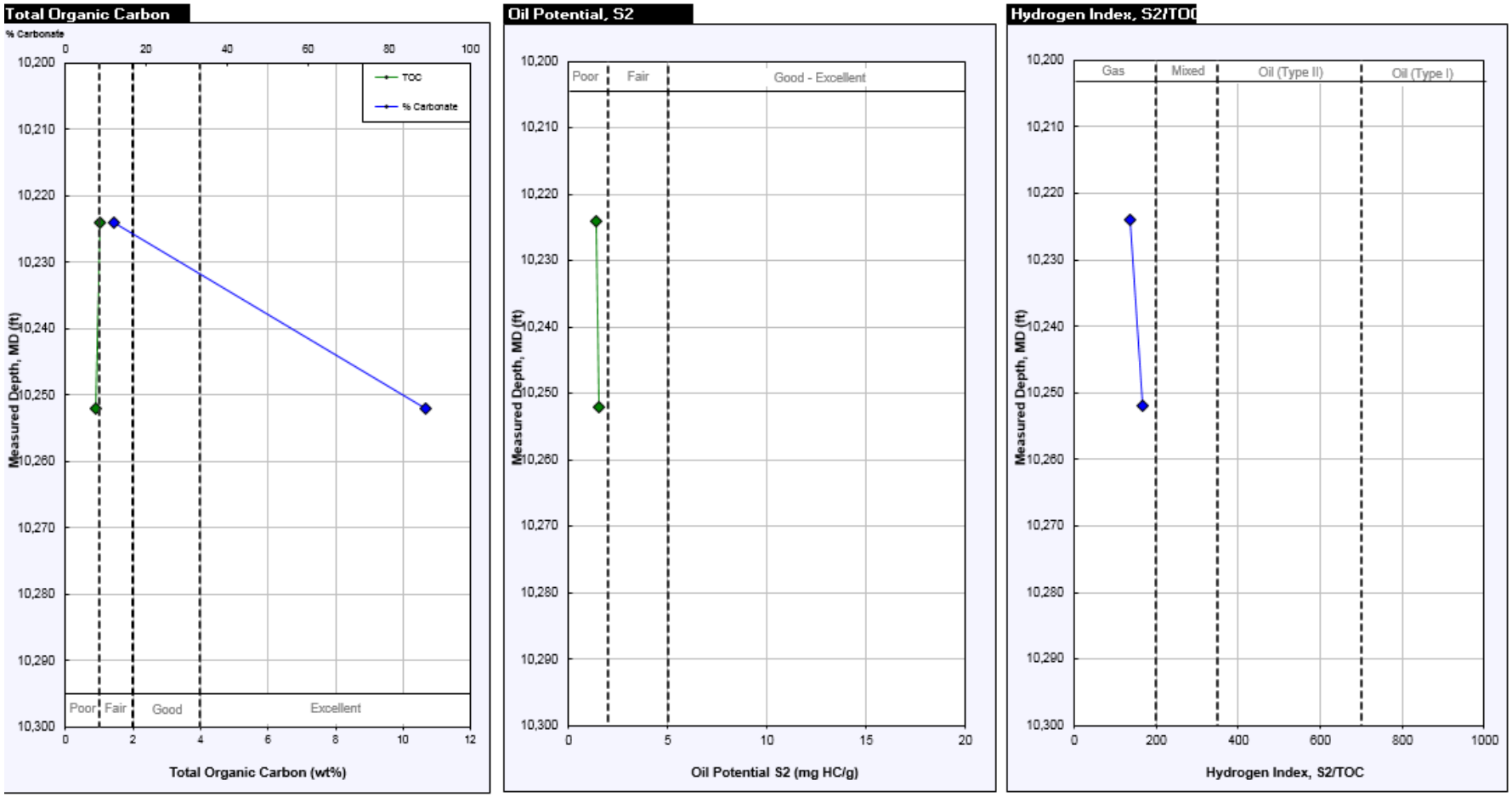

Figure 4-8: Source potential logs for Second Bone Spring Sand

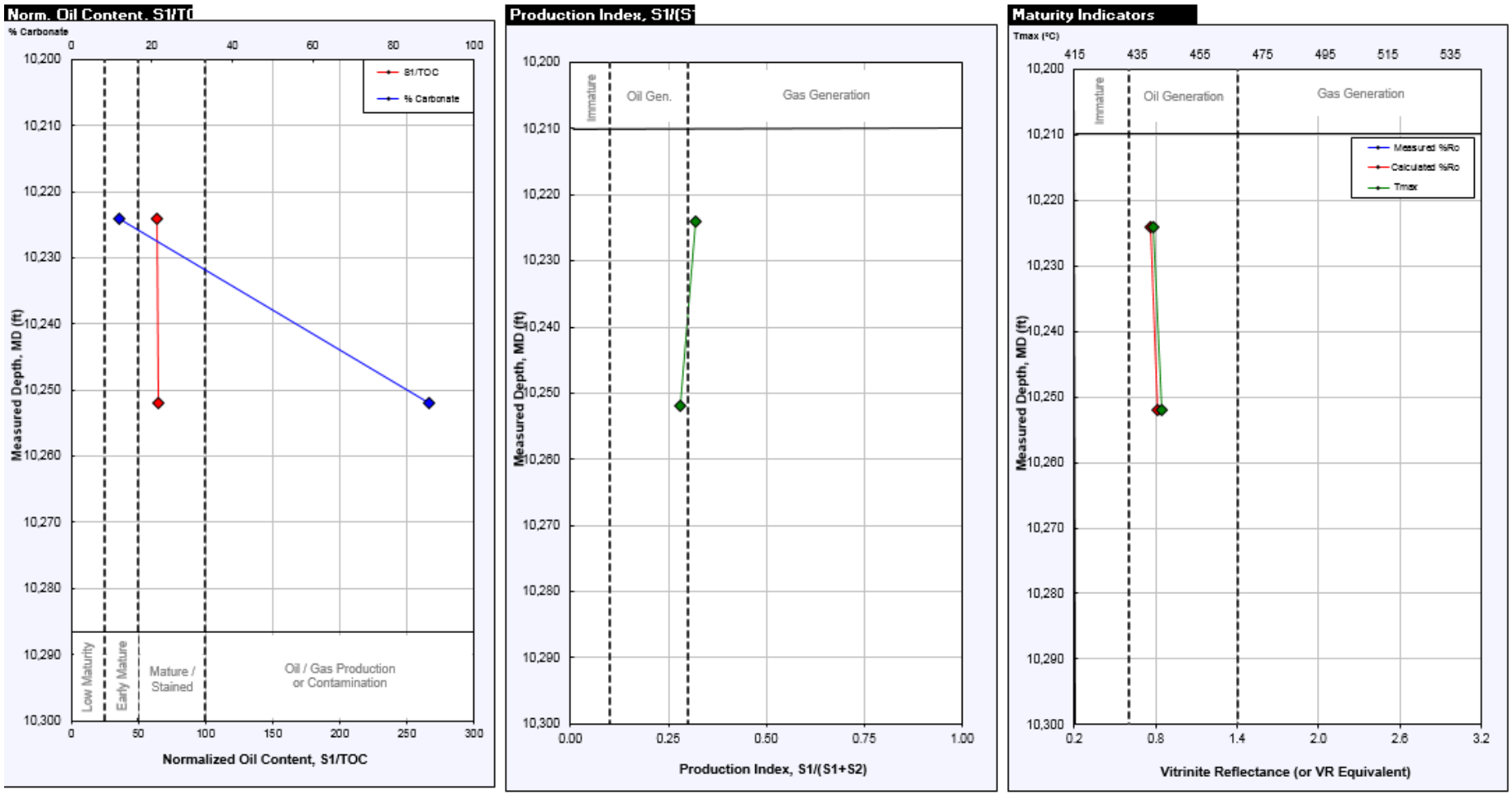

Figure 4-9: HC indicator and maturity logs for Second Bone Spring Sand

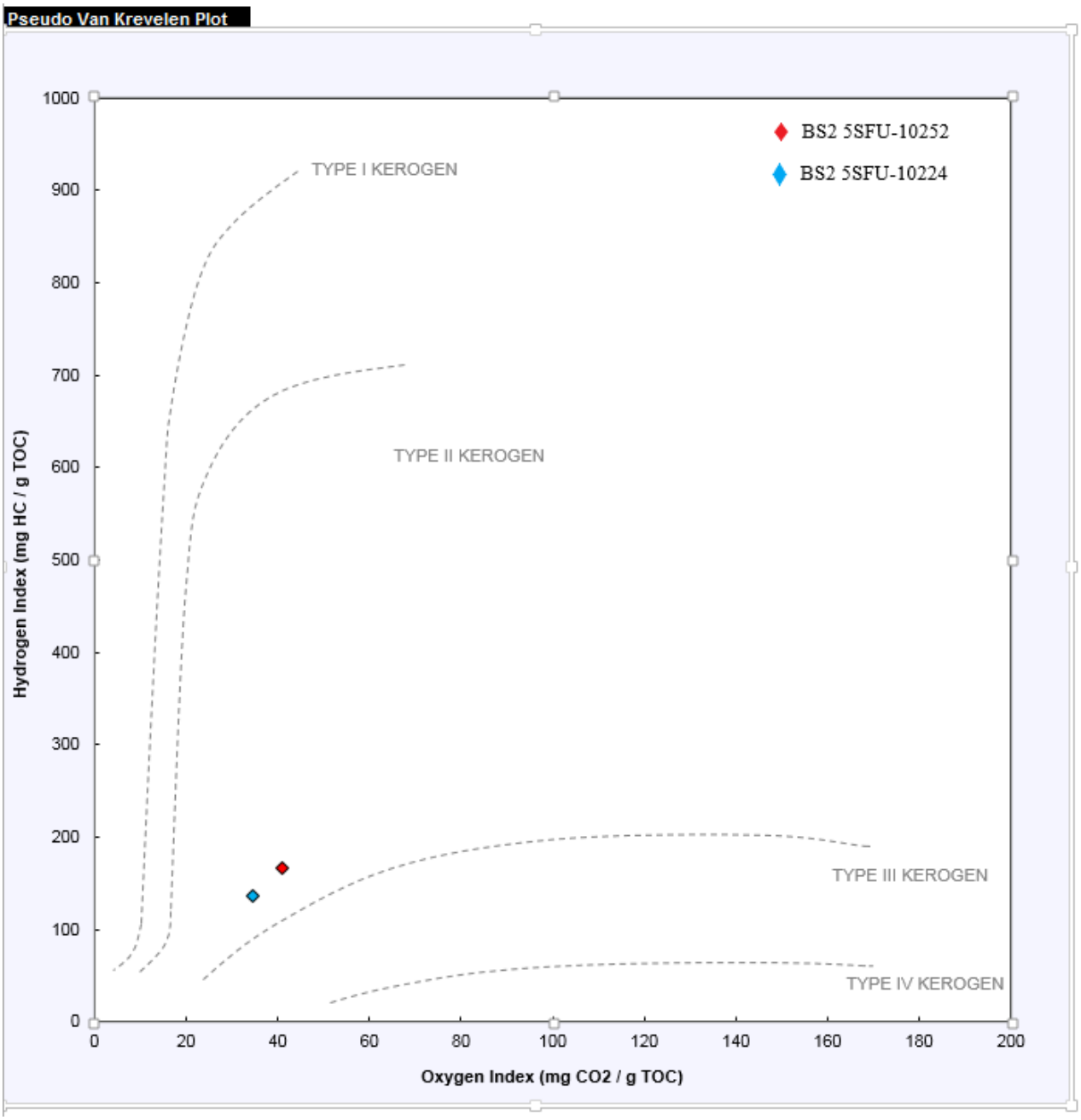

Figure 4-10: Pseudo Van Krevelen Plot for Second Bone Spring Sand

4-3 Vacuum Saturation

Table 4-4

Edge accessible porosity results from vacuum saturation

	DI Water						
	Cubes			Plugs			
Sample ID	Porosity (%)	Bulk density (g/cm3)	Grain density (g/cm3)	Porosity (%)	Bulk density (g/cm3)	Grain density (g/cm3)	Porosity difference (%)
AS 1AF-6298	0.404	2.669	2.680	3.736	2.651	2.754	-824.75
AS 1AF-(6328-6331)	6.742	2.496	2.677				
AS 1AF-6342	1.833	2.532	2.579	4.26	2.521	2.633	-132.41
AS 1AF-6384	0.575	2.625	2.64	3.799	2.582	2.684	-560.7
BS1 3PF-6147	8.12	2.49	2.682				
BS2 5SFU-10224	2.985	2.539	2.738				
BS2 5SFU-10243	0.774	2.734	2.755				
BS2 5SFU-10252	0.654	2.793	2.811				

Table 4-4 presents the vacuum saturation results for Avalon Shale, First and Second Bone Spring Sands. Twenty-four cubes and twelve core plugs from three wells across the Bone Spring formation were analyzed for the edge-accessible porosity using the vacuum saturation technique. Porosity, bulk density and grain density values in column two, three and four respectively represent the average values for each sample. Three cube samples from each depth were used in conducting this experiment, while columns five, six and seven represents average values obtained from twelve Avalon Shale core plugs only. Samples AS 1AF-6298, AS 1AF-6342 and AS 1AF-6384 had four, five and three plugs respectively. Results show that sample AS 1AF-96328-6331) is more porous for the cube samples, whereas sample AS 1AF-6298 is the least porous. Both porosity and density results show no discernible trends, but it is evident that the largest porosity and smallest bulk density readings came from the plugs. The porosity difference (%) among the two methods is displayed in column eight.

Negative sign is an indication that the porosity value has increased from the first porosity reading, and this may be attributed to the presence of fractures within the plug sample.

4-4 Core Porosity and Permeability

Table 4-5
Helium porosity and permeability results for Avalon Shale

Sample ID	Depth (ft.)	Caliper Bulk Vol (cm^3)	Dry Weight (g)	Grain Density (g/cm^3)	Pore Vol (cm^3)	Porosity (%)	Air Permeability k_{air} (md)
AS 1AF-6298 Parallel 1	6298	19.703	52.57	2.677	0.069	0.35	0.218
AS 1AF-6298 Parallel 2	6298	19.052	50.35	2.682	0.278	1.459	0.317
AS 1AF-6298 Transverse 1	6298	8.561	22.66	2.706	0.1875	2.190	
AS 1AF-6298 Transverse 2	6298	6.893	18.27	2.680	0.077	1.117	
AS 1AF-6342 Parallel 2	6342	6.116	15.6	2.567	0.0385	0.630	
AS 1AF-6342 Transverse 2	6342	8.68	21.68	2.554	0.1885	2.172	0.00011
AS 1AF-6342 Transverse 3	6342	10.038	25.33	2.5365	0.0525	0.523	
AS 1AF-6384 Parallel	6384	6.17	15.7	2.6075	0.15	2.431	
AS 1AF-6384 Transverse 1	6384	15.418	40.35	2.6395	0.1305	0.846	0.00076
AS 1AF-6384 Transverse 2	6384	16.21	42.25	2.6275	0.1315	0.811	0.00069

This test was performed at the Oil and Gas Survey of China Geological Society with UltraPore-300 and PDP-200 (Core Laboratories). The measured air permeability and calculated porosity values for Avalon shale are displayed in Table 4-5. Well samples not included in the test were excluded as they didn't meet the needed sample size. Ten parallel and transverse plugs from Avalon Shale were used in calculating the plug porosity. Air permeability test was done for five core plugs.

Results indicate that the calculated porosity values for Avalon Shale, ranging from 0.35% (in sample AS IAF-929 parallel 1) to 2.43% (in sample AS IAF-6384 parallel). Air permeability values for Avalon Shale range from 0.00011 md to 0.32 md. First Bone Spring Sand porosity and permeability data from Saga Petroleum Corporation are displayed in Figure 4-6. The report shows that porosity is 8.1% at depths of 6146.9 feet, 9.2% at 6256.2 feet, and 8.8% at 6257.9 feet. Equally, air permeability values for those depths are 0.041 md, 0.063 md and 0.065 md, respectively.

Table 4-6

First Bone Spring Sand porosity and permeability result (Saga Petroleum Corp.)

Formation	Depth (ft.)	k_{air} (md)	Porosity (%)	Grain density (g/cm^3)
1^{st} Bone Spring sand	6146.9	0.041	8.1	2.67
	6256.2	0.063	9.2	2.71
	6257.9	0.065	8.8	2.68

4-5 Mercury Injection Capillary Pressure (MICP)

The MICP is a technique capable of generating varieties of petrophysical data from a single theoretical model (Webb, 2001). Gao and Hu (2013) have shown that the MICP test can provide useful insights into bulk density measurement, total pore area, porosity, total pore area, median pore throat size, pore throat size distribution, and permeability. Table 4-7 below is the derived and calculated MICP result for Avalon Shale, First and Second Bone Spring Sands, whereas Figure 4-11 represents the pore-size distribution for the test samples. Figure 4-11 will help in identifying the common pore types available in the respective samples, whereas the pore volume in each sample is displayed in Figure 4-12.

Table 4-7

Summary of MICP results

Sample ID	Bulk density (g/cm^3)	Total pore area (m^2/g)	Porosity (%)	Median pore throat diameter (by area) (nm)	Median pore throat diameter D50 (by volume) (nm)	Permeability (md)	Tortuosity (D_o/D_e)
AS 1AF-6298	2.665	0.006	0.204	189	1,719	1.78E-02	5.27
AS 1AF-(6328-6331)	2.487	2.900	5.844	16.3	68.3	2.05E-03	3.77
AS 1AF-6342	2.544	0.001	0.2687	968	32,977	12.3237	3.69
BS2 5SFU-10224	2.549	2.534	2.6298	9.57	22.01	5.23E-06	7.30
BS2 5SFU-10243	2.746	0.217	0.4287	12.99	52.39	8.85E-01	3.51
BS2 5SFU-10252	2.787	0.021	0.2671	58.52	2,873	3.95E-03	4.78

The graph in Figure 4-11 show that both samples AS 1AF-6298 and AS 1AF-6342 have no mercury intrusion in pores less than 0.1 μm. The absence of the lower pores impacts the average permeability value for each sample, and this may be responsible for the high permeability readings obtained. Samples AS 1AF-6298 and BS2 5SFU-10252 both have similar mineralogical composition, therefore the presence of fractures within AS 1AF-6298 and AS 1AF-6342 may be responsible for lack of mercury intrusion at pores smaller than 0.1 μm. Tortuosity (a measurement of how complex the pore structures are) values for the tested samples range from 3.51 to 7.29.

Pore types are synonymous with pore throat diameter (Hu et al., 2017), and they include inter-clay platelet (0.0028-0.005 μm), organic pores (mostly 0.005-0.01 μm), intragranular pores (mostly 0.01-0.05 μm), intergranular pores (mostly 0.05-0.1 μm), and microfractures (0.1-50 μm). The test results (Figure 4-11) show that microfractures are the dominant pore type amongst the organic, intragranular, and intergranular pore spaces found within the Avalon Shale. Microfractures and intragranular pore spaces are the two most common pore types found within the Second Bone Spring sand. Generally, of all samples tested, microfractured pore spaces are the most abundant-pores, while inter-clay platelet pores are the least common pore types.

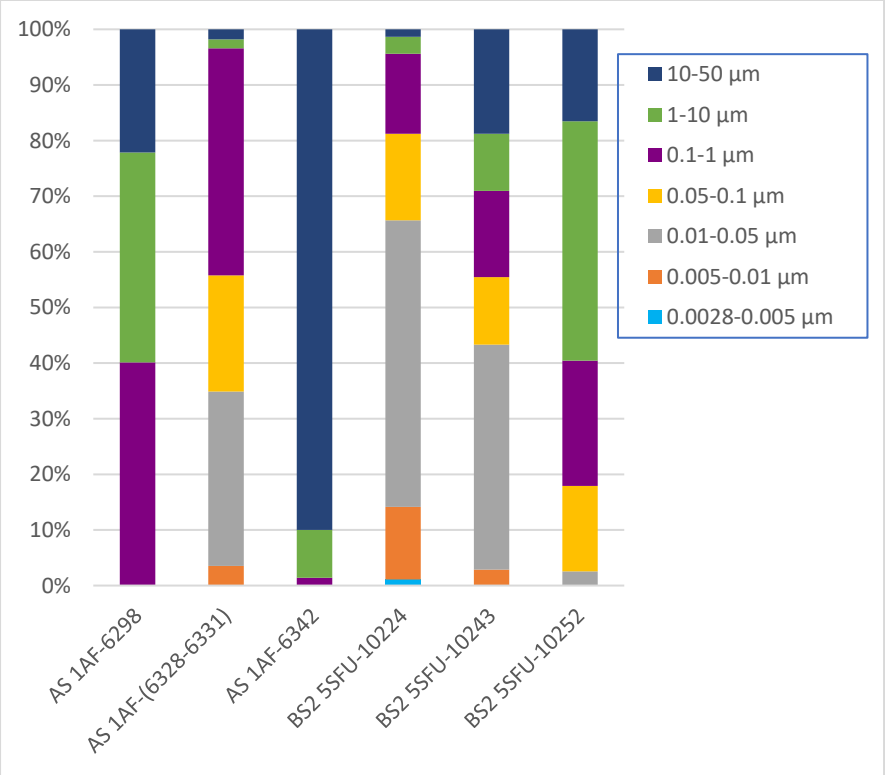

Figure 4-11: Pore throat size distribution for Avalon Shale and Second Bone Spring Sand

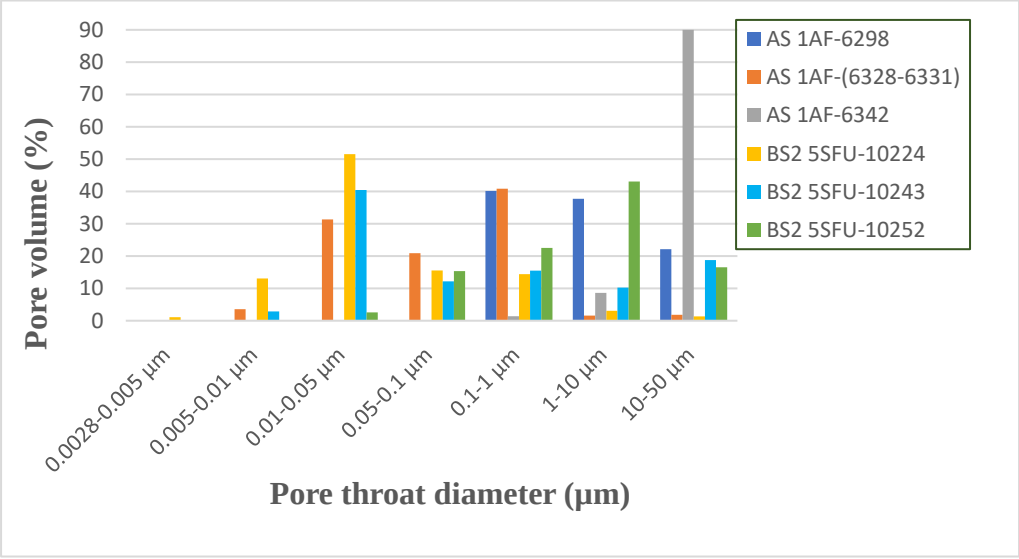

Figure 4-12: Volume of pore throat diameter from Avalon Shale and Second Bone Spring Sand

4-6 Density measurements

Table 4-8

Apparent bulk density results from Archimedes displacement and pycnometry tests

	Archimedes Displacement	Pycnometry Test					
		DI water			DT2		
Sample ID	Cube	GRI+	GRI	Size C	GRI+	GRI	Size C
AS 1AF-6298	2.684	2.674	2.663	2.541	2.712	2.644	2.543
AS 1AF-(6299-6300)		2.633	2.617	2.433	2.631	2.619	2.483
AS 1AF-(6328-6331)	2.538						
AS 1AF-6342	2.533	2.572	2.481	2.511	2.603	2.548	2.475
AS 1AF-6384		2.627	2.61	2.475	2.669	2.653	2.615
BS1 3PF-6147	2.536						
BS1 3PF-6257		2.643	2.629	2.536	2.660	2.641	2.512
BS2 5SFU-10224	2.570	2.628	2.597	2.575	2.621	2.528	2.528
BS2 5SFU-10243	2.749						
BS2 5SFU-10252	2.789						

Table 4-8 displays the apparent bulk density results from Archimedes displacement and pycnometry tests. Ninety-three samples comprising twenty-one cubes and seventy-two sieve fractions (GRI+, GRI and size C) were tested. DI water is the immersion fluid for Archimedes displacement test, whereas both DI water and DT2 solution (a mixture of n-decane and toluene in the volumetric ratio of 2:1) were used for the pycnometry experiment. Cube-sized samples were used for the displacement test, whereas the pycnometry test was conducted with the sieve fractions. Column 1 in Table 4-8 above represents sample horizons, and it is important to note that not all samples were represented in all experiments.

The most common trend observed from the results is the decrease in bulk density as the sample size (sieve fraction) decreases from GR+ to size C, irrespective of the immersion fluid used during the experiment. The only exception is the DI water (GRI result) for sample AS 1AF-6342, with a much smaller bulk density among the three sieve sizes. Generally, bulk density is known to correlate negatively with porosity (Shakir et al., 2002) and the grain density among size fractions is similar, therefore it is expected that the smaller the sample size, the higher the porosity values obtained. The Archimedes displacement results for the cube samples show no correlation with the pycnometry results, as some of the bulk density results were larger and some smaller than the sieve fractions.

4-7 Spontaneous Imbibition

The imbibition slopes in Figure 4-13 and Figure 4-14 represent the sample's behavior when in contact with DI water or DT2 solution. Multiple runs were performed to ensure consistency and to reduce errors. The slopes are plotted as a product of logarithmic time (minutes) against the logarithmic cumulative imbibition height, bearing in mind that the square root of the imbibition time is proportional to total volume of imbibed fluid (Yang et al., 2017). Three slopes (Slope I, II III) obtained from experiments represent the different stages as the fluid migrates to the sample top. Slope I is first stage

and represents the behavior of the sample the moment it touches the fluid; this slope is shown in brown and it lasts between few seconds to one minute, before the start of the second stage. Slope II represents the initial fluid migration to the contact surface, and this slope lasts up to about 45 minutes. Slope values for the stage II are mostly larger as the edge accessible pores get invaded. The third stage (Slope III), also known as the connectivity slope, is the most important of all and it represents the behavior within the rock matrix. This is consistent with the pore connectivity and wetting. This slope extends till the end of the experiment and is displayed in red. The Stage IV slope associated with the DT2 solution is painted in blue exists when the fluid reaches the sample top.

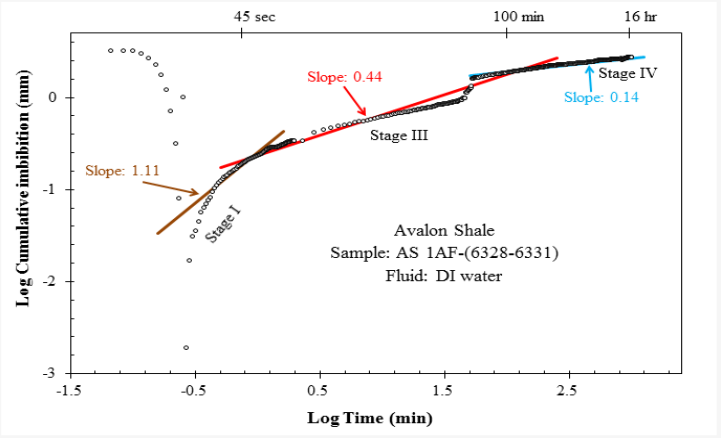

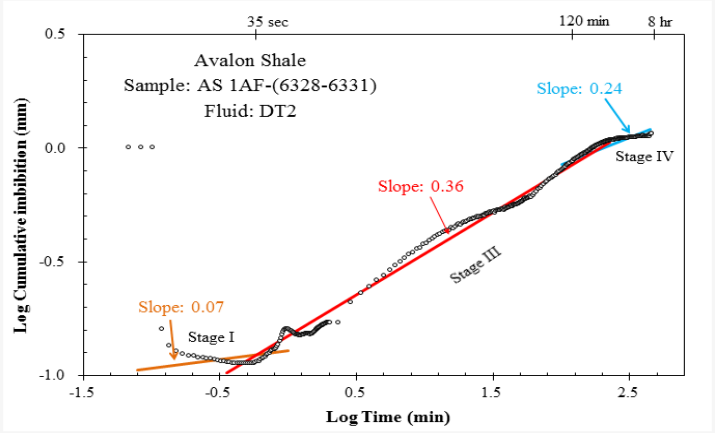

Figure 4-13: DI water and DT2 imbibition slope for Avalon Shale (AS 1AF-(6328-6331))

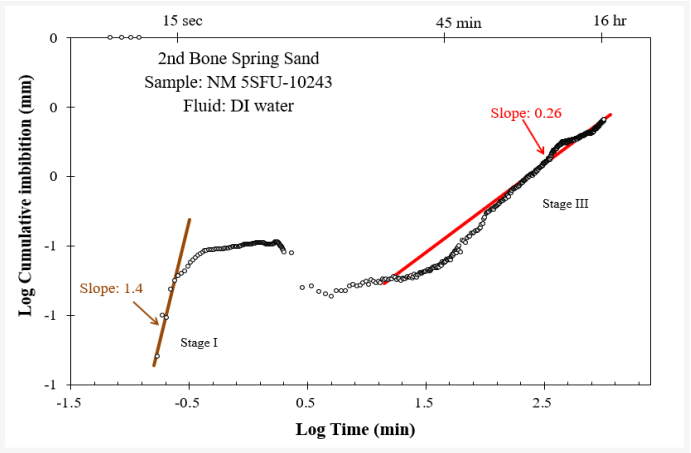

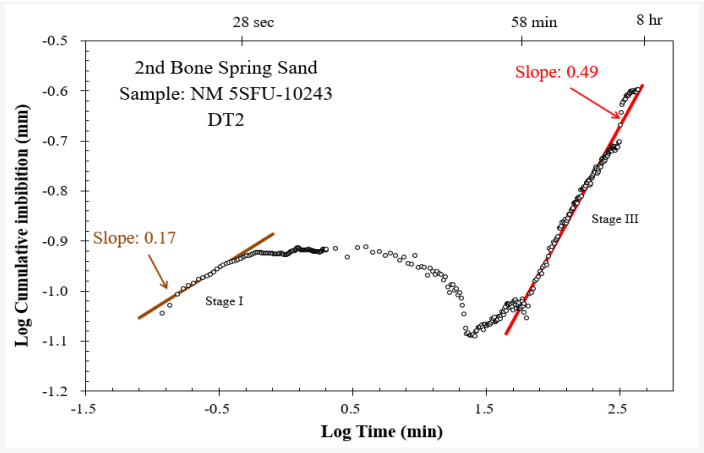

Figure 4-14: DI water and DT2 imbibition slope for Second Bone Spring sample (BS2 5SFU-10243)

Table 4-9 below has the summary of the calculated imbibition slopes for Avalon Shale, First and Second Bone Spring Sands. The connectivity slope (Slope III) with values approximately equal to 0.5 indicate a well-connected pore network (i.e., the square-root-of-time relationship in log-log plot of imbibed fluid amount vs. time) for the fluid in question. Results show that sample AS 1AF-6342 and AS 1AF-6384 of the Avalon Shale exhibit high connectivity for water wetting fluid, whereas sample BS2 5SFU-10243 of the Second Bone Spring Sand displays a high connectivity for the oily fluid of DT2. Slope III values between 0.5 and 0.26 equates to intermediary wet samples, whereas values less than 0.26 is equivalent to samples with low connectivity for the fluid.

Table 4-9

Imbibition slopes for DI water and DT2

Sample ID	Fluid	Slope I	Slope II	Slope III	Slope IV
AS 1AF-6298	DI water	0.757	0.259	0.351	x
	DT2	x	x	x	x
AS 1AF-(6328-6331)	DI water	1.11	x	0.442	0.143
	DT2	0.075	x	0.361	0.068
AS 1AF-6342	DI water	0.845	0.068	0.5	x
	DT2	x	x	x	x
AS 1AF-6384	DI water	0.247	0.126	0.59	x
	DT2	x	x	x	x
BS1 3PF-6147	DI water	0.021	0.077	0.377	x
	DT2	x	x	x	x
BS2 5SFU-10224	DI water	0.923	0.079	0.269	x
	DT2	x	x	x	x
BS2 5SFU-10243	DI water	1.404	0.06	0.255	x
	DT2	0.167	-0.06	0.486	x
BS2 5SFU-10252	DI water	0.571	0.337	0.209	x
	DT2	x	x	x	x

4-8 Well Production Data

Production data and well information summarized below were obtained from DrillingInfo, while additional data was sourced from New Mexico Oil Conservation. Well data consists of completion date, target reservoir, well test date, date of first production, last production date, monthly production, cumulative production, total depth, true vertical depth, elevation, trajectory, field name and formation tops. Table 4-10 is the summary of production data for the three wells used in this research.

Avalon Shale was cored from well Amoco Federal 11 #001, located in Eddy County of New Mexico. Its spud date was August 4th, 1979, first completion date was August 8th, 2002 and the target reservoir was the Brushy Canyon (East). This active and oil producing vertical wellbore has a total depth and true vertical depth of 11900 feet. Upper and lower perforations were done at 4759 feet and 4791 feet, respectively. Additional data from New Mexico Oil Conservation show that the formation top for Delaware Mountain Group is at 2690 feet, Brushy Canyon formation at 4750 feet, Bone Spring formation at 6230 feet, first Bone Spring Sand at 7330 feet, and the Wolfcamp at 9675 feet.

First Bone Spring Sand was cored from well Potts Federal #003, located in Eddy County of New Mexico. The currently active well was completed in June 21, 2003. Production began on July 1st, 2003 and the target play was the Morrow formation. This vertical wellbore has an elevation of 3320 feet, a total and true vertical depth of 11253 feet. Upper and lower perforations were located at 11124 feet and 11132 feet, respectively. Formation tops obtained from New Mexico Oil Conservation show that the Delaware sits at 3030 feet, Bone Spring Formation at 4556 feet, 1st Bone Spring Sand at 6144 feet, and top of the Wolfcamp at 9455 feet.

Second Bone Spring Sand was cored from well State FU #005, located in Lea County of New Mexico. This well has been plugged and abandoned (P&A) since October 27, 1993. Its first production date was on July 1st, 1983 while the last production was on November 1st, 1988. This vertical wellbore has a total and true vertical depth of 10900 feet, elevation is 3971 feet and the target reservoir is the

Bone Spring. Data from New Mexico Oil Conservation show that the Delaware Formation top is at 5940 feet, Bone Spring Formation top is at 7832 feet, first Bone Spring Sand is at 9103 feet, second Bone Spring Sand is at 9460 feet, and the third Bone Spring Sand at 10296 feet.

Table 4-10

Production data for Amoco Federal 11 #001, Potts Federal #003 and State FU #005 wells

Well Name	County	Field	Reservoir	Play Name	Cum. Oil (BBL)	Cum. Gas (Mcf)	Status
Amoco Federal 11 #001	Eddy	Loving	Brushy Canyon, East	Avalon Shale	174311	456668	Active
Potts Federal #003	Eddy	Burton Flat; Morrow	Morrow	First Bone Spring Sand	-	309200	Active
State FU #005	Lea	Airstrip	Bone Spring	Second Bone Spring Sand	170010	145397	P & A

Chapter 5

Discussion

The production of unconventional reservoirs face unique challenges, and this research demonstrates the importance of critical petrophysical properties like porosity, permeability, total organic carbon, kerogen maturity, imbibition characteristics, bulk density, and mineralogy. It is important to note that several re-runs were performed in most cases, to help minimize errors from data collection. Further discussion is carried out under the following sub-headings of production potential, porosity/permeability, pore network and fluid flow.

5-1 Production Potential

The production potential of tight oil formations is dependent upon the quality of the reservoir, and the success of the fracture stimulation (Britt and Schoeffler, 2009). The geochemical result suggests that there is a significant resource within the Avalon Shale, while the optimal landing zone can be identified with the help of the petrophysical log (Figure 5-1). A further consideration in this section will only be given to sample AS 1AF-6342 of the Avalon Shale, as other samples fell short of the criteria discussed below.

Laboratory tests show~~s~~ that sample AS 1AF-6342 of the Avalon Shale has a high TOC value of 2.25% and a T_{max} (438^{o}C) that falls within the oil window. Elevated TOC levels exceed the average value for shale source rocks (2.2%; McDade et al., 1993), suggests that the Avalon Shale is a source rock. Source potential logs (S2 value of 4.76 mgHC/g) indicates a moderate hydrocarbon generating potential that conforms to Peters (1986) assertion, that S2 values less than 0.2 are very unreliable irrespective of the T_{max}. Pseudo Van Krevelen plot and the kerogen quality plot indicate a type II/III kerogen (marine and terrestrial origin), thus suggesting that sample AS 1AF-6342 of the Avalon Shale is oil and gas prone.

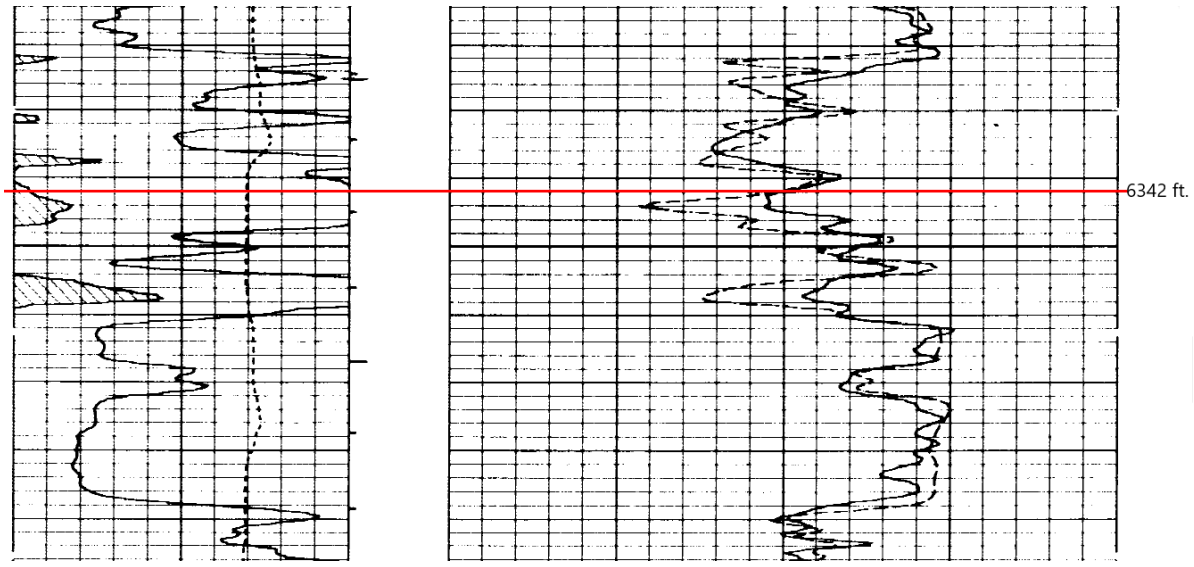

Figure 5-1: Amoco Federal 11 well log showing log traces at horizon 6342 feet. The density and porosity cross-over in track 2 suggests a good landing zone and it is in harmony with pyrolysis and TOC results for sample AS 1AF-6342 of the Avalon Shale (modified from New Mexico oil Conservation)

Despite good geochemical results for sample AS 1AF-6342, the percentage of quartz to clay may provide important details regarding the ease of recovery (Harris et al., 2011). To maximize recovery, a knowledge of the lithology is needed in order to design the right kind of fracture (NRC, 1996). High quartz intervals with a small percent of clays responds better during hydraulic fracturing (Berskin et al., 2001). Clay-rich rocks (between 26% - 88% clay) are ductile and incapable of developing fracture permeability (Ingram and Urai, 1999). Figure 5-2 is the XRD result for sample AS 1AF-6342 with 53.5% quartz, 24% carbonate and 22.5% clay, which suggests an optimum balance for good fracture growth.

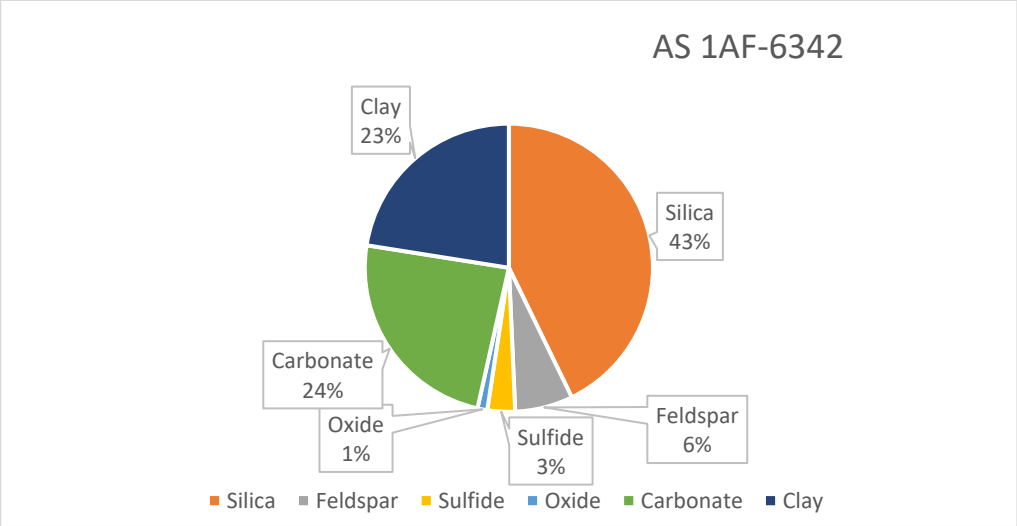

Figure 5-2: XRD result for sample AS 1AF-6342

5-2 Porosity and Permeability

Porosity is the ratio of the void spaces to the total bulk volume of a given material, while permeability on the other hand measures the ability of a porous media to transmit fluid. Quantifying porosity and measuring permeability of tight formations is a critical step in reservoir quality estimation, because a significant percent of total gas exists as absorbed gas (Bustin, 2006). The inconsistent porosity results obtained from different experiments is largely due to sample size differences, and fractures become more pronounced in larger samples than in the smaller samples. An occurrence of type II/III kerogen in the Avalon Shale suggests that matrix permeability might be affected by the co-presence of oil and gas. In general, the low porosity values from vacuum saturation, MICP and core plug experiments suggests that microstructures, clay composition or maturity may be a major factor.

Figure 5-3 below suggests that there is a close relationship between the clay composition of some samples and the occurrence of intergranular (0.05-0.1 µm) and intragranular (0.01-0.05 µm) sized pores. The samples with higher clay content have these pores in abundant, whereas sample AS 1AF-6342 of the Avalon Shale and BS2 5SFU-10252 of the Second Bone Spring Sand are the only

exception. It is important to note that sample BS2 5SFU-10243 (with the red arc in Figure 5-3) has no XRD results. Further analysis shows that sample AS 1AF-6342 of the Avalon Shale with 23% clay is dominated by microfracture sized pores (0.1-50 µm), and as such at odds with Villagas (2016) findings in Niobrara Shale. Villagas advocated that a higher clay content results in increased presence of intragranular and intergranular pores, which affects porosity. Sample BS2 5SFU-10252 with 0% clay has the intergranular and intragranular pores, unlike sample AS 1AF-6298 with 23% clay. The absence of the smaller sized pores (<0.1 µm) in sample AS 1AF-6342, can be attributed to the effect of compaction. The chart in Figure 5-4 shows that sample AS 1AF-632 is rich in TOC, but has the least maturity of all samples tested. The correlation between TOC and T_{max} showed no pattern, but in Figure 5-5, the smaller pores are present on samples with higher maturity.

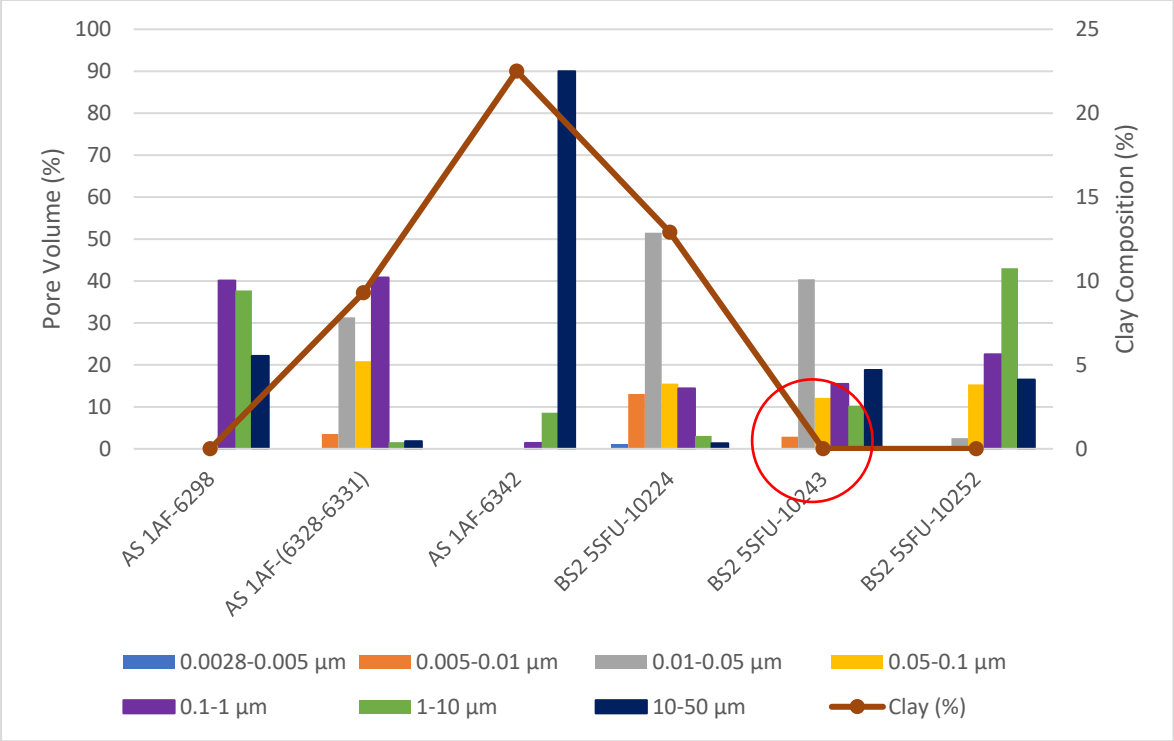

Figure 5-3: Pore size distribution against clay composition for Avalon Shale and Second Bone Spring Sand. Red arc indicate Bone Spring sample without an XRD result.

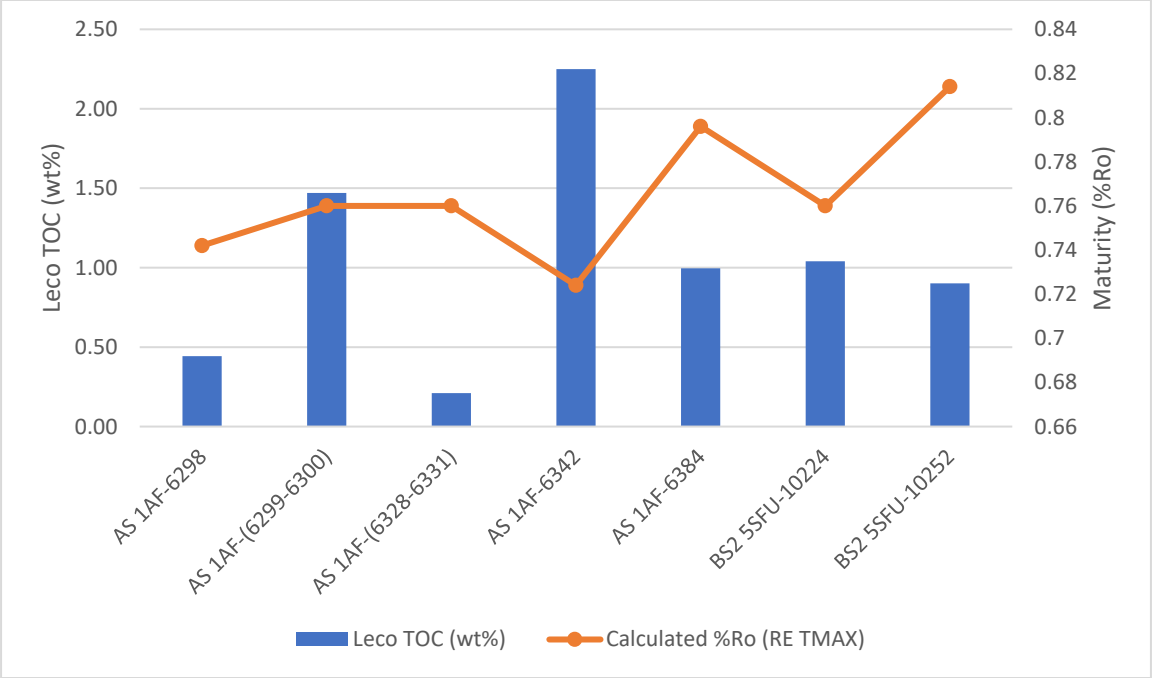

Figure 5-4: Leco TOC plotted against sample maturity (RE T_{max})

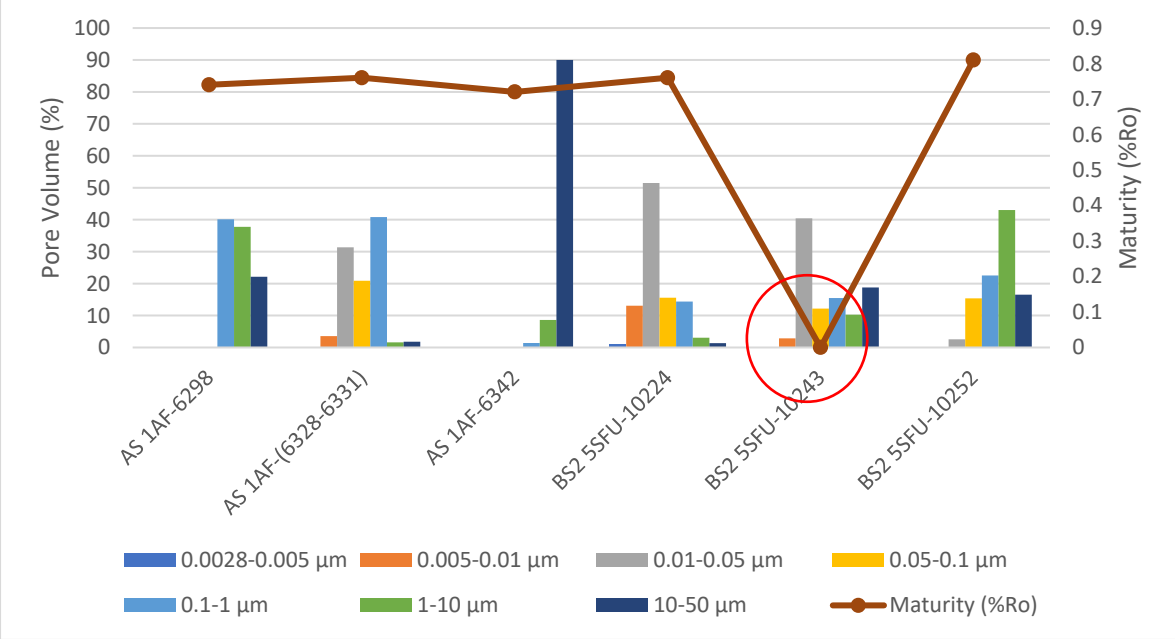

Figure 5-5: Pore size distribution against maturity (%Ro) for the Avalon Shale and Second Bone Spring Sand. Red arc indicate sample without a pyrolysis result.

Figure 5-6 compares sample's porosity with clay composition. The absence of clay-sized particles may preserve interparticle porosity among samples with interplatelet pores (0.0028-0.005 µm), thus suggesting that clay is responsible for the low porosity in sample AS 1AF-6342 as compaction takes place. Additionally, the samples with higher porosity in Figure 5-6 are the samples (AS 1AF-(6328-631) and BS2 5SFU-10224) with higher percentage of intragranular pore sizes (0.01-0.05 µm) and very low microfracture pores greater than 1 micrometer (>1 µm). Sample BS2 5SFU-10243 of low porosity has a greater percentage of pores sizes greater than 1 µm. Figure 5-7 compares the effect of carbonate composition to pore size distribution, and no correlation was found.

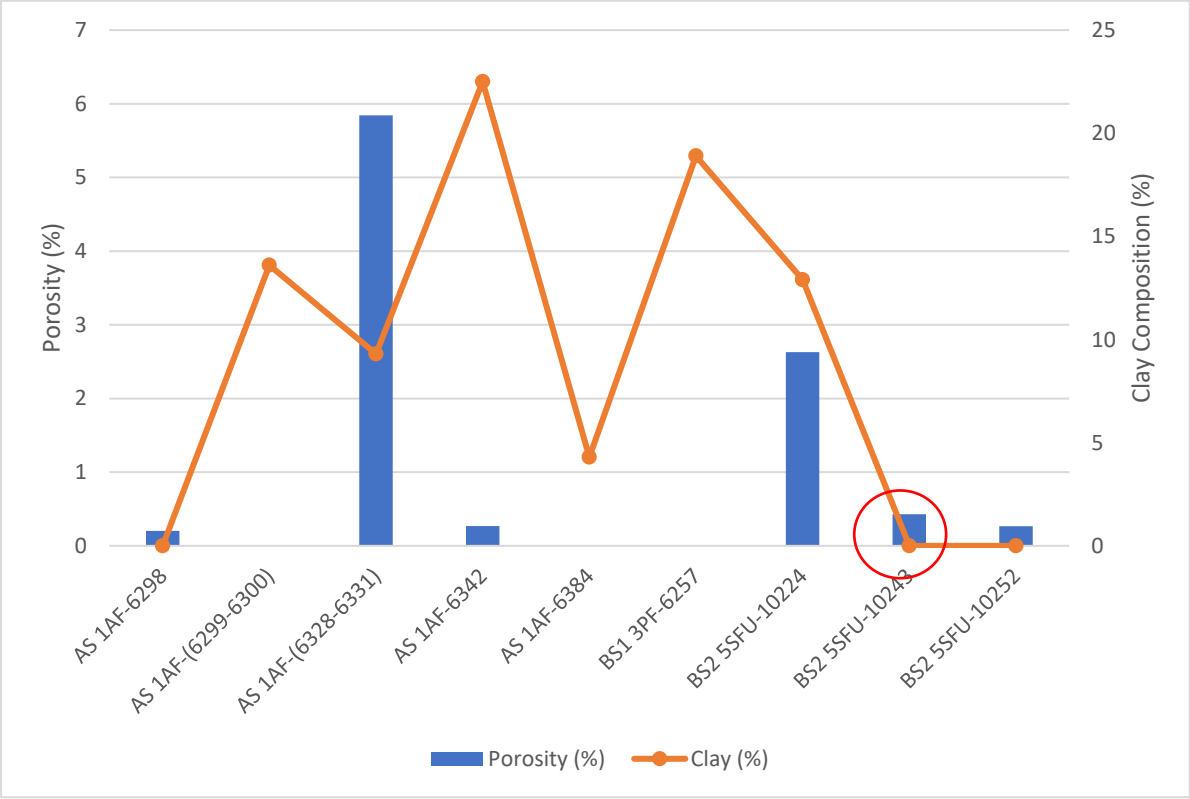

Figure 5-6: MICP porosity against clay contents in Avalon and Second Bone Spring Sands. Red arc indicate sample without an XRD result.

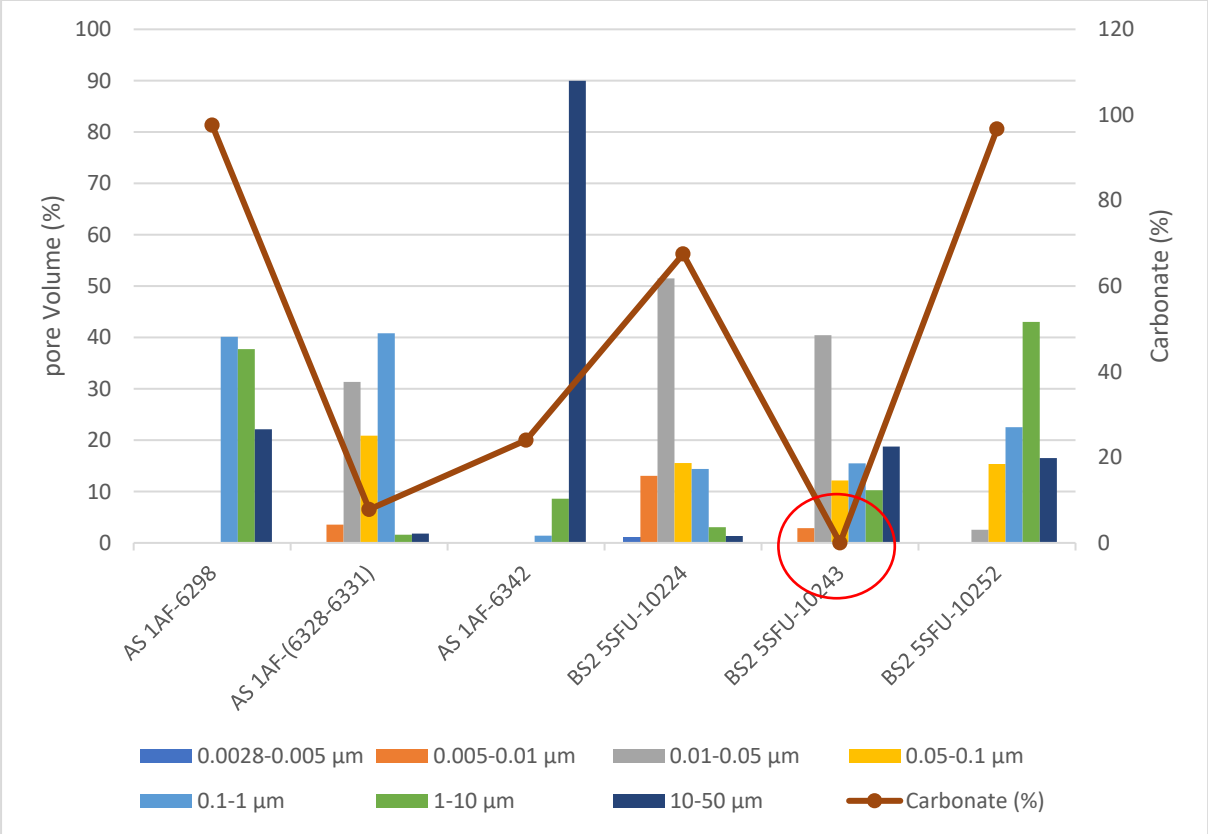

Figure 5-7: Pore size distribution against carbonate composition for Avalon and Second Bone Spring Sand. Red arc indicate sample without XRD results.

Chapter 6

Conclusion and Recommendation

Low porosity and permeable reservoirs pose measurement challenges, and for a better understanding, various laboratory experiments have successfully been carried out. Results indicate that the Avalon Shale has a moderate hydrocarbon generating potential, with sample AS 1AF-6342 having an S2 value of 4.76 mgHC/g, TOC value of 2.25%, T_{max} value of 438^{o}C, is oil prone and rich in type II/III kerogen (marine and terrestrial origin). Average TOC content across the Avalon shale stands at 1.1%, and 0.97% for the Second Bone Spring Sand. XRD results indicate the existence of five different lithofacies within the Avalon Shale and two among the Bone Spring Sands. Average porosity for Avalon Shale range from 0.2 to 6.7%, 4.9 to 8.1% for the First Bone Spring Sand, and 0.3 to 3% for the Second Bone Spring Sand. Permeability is very low and will be affected by the co-presence of oil and gas within the Avalon Shale. MICP results show that organic, intragranular, intergranular and microfracture pores, are common pore types found within the Avalon Shale, whereas inter-clay platelets, organic pores, intragranular, intergranular and microfractures are found in the Second Bone Spring Sand. Spontaneous imbibition results show that the Avalon Shale is moderately to water wet, intermediary wet for First Bone Spring Sand and Oil wet for the Second Bone Spring Sand. Pore structure characteristics show that clay composition, compaction and the ratio of intragranular sized pores to microfractures greater than 1 micrometer, all affects porosity. The higher the microfracture-sized pores greater than 1 micrometer, the lower the porosity.

The results from this study recommend targeting the source rock at 6342 feet for horizontal drilling, as it has the optimal mineralogy to maintain a good fracture growth. Furthermore, the overlying rocks at 6328-6331 feet are porous, rich in quartz and will support a good fracture height.

Chapter 7 - Appendix

Appendix A: Shimadzu Center Standard Operating Procedure for XRD Analysis

MaximaX XRD-7000: Shimadzu X-ray Diffractometer

Preparation of sample

- Use a glass slide to compact your sample in the sample holder.
- With the help of the glass slide edge, remove the excess sample, to avoid vertical loading.
- Try and ensure your sample is homogeneous and flat as much as possible. You can now analyze your sample after making it completely flat and homogeneous.

Power settings

- Press the power button that is placed on the face of the chiller, to turn on the chiller. A green light illumination shows the chiller is on.
- Before you proceed to adjust the appropriate temperatures, give the chiller around 20 minutes after switching on.
- Now press the power button that is on the left-hand side of the chiller, so as to turn the XRD on. The XRD front panel will be illuminated by the green power button.

Calibrating the XRD

- On the desktop, look for [PCXRD] program and launch it. The action makes the primary "XRD-6100/7000" panel to display.
- Now click the (setup and display) button. This opens up a "door alarm check" window. For the XRD door to open, follow the prompt instructions. Once the door opens, click the "Close" button. After closing, an "Icon" window pops-up displaying the message "Now Calibration! If ready Ok." Click the "OK" button.

- By doing so, you have already calibrated the XRD, and you can now start analyzing your sample.

How to set specifications of analysis

- To set up the analysis specifications, move to the "XRD 6100/7000" panel.
- Click the "Right Gonio Condition" button, to open the "Edit Program" window.
- Under the "Measurement Mode: Standard" select the blue bar, so that you can expand the "Standard Condition Edit" window.
- In the window, you will find most settings are already preset, and you only need to change a few conditions.
- Here is the general condition setting that functions for a wide variety of materials. It is worth mentioning that following these steps is crucial. To ensure you are following the guidelines precisely, ensure you have double checked any settings that you have changed. By doing so, you will have protected the detector from damage, as well as minimizing small mistakes when you are analyzing materials.
    i. Scanning condition: The scan range in degrees is 2°-70°. For optional condition, check the "Option Enable" box.
    ii. Beta attachment: select control mode, and set the speed of rotation as 6rpm.
    iii. Slit condition: The condition get preset, but you must verify it on the XRD, so that you are sure the appropriate slit sizes fit the settings specified under the conditions.

    How to check the slits:

    - Upon opening the XRD door, check the X-ray tube on the left of the XRD. On the left of divergence soller slits, you will find the Divergence slit attached.

- The detector arm is on the right side. The arm comprises of scattering slit, facing the sample on left, the receiving slit, facing the detector on right and a set of scattering soller slits.
- If the slits are of different sizes with the "Slit Condition" box presets, ensure you have matched the slits by changing them.

iv. Settings of standard slits:

- Set the divergence slit to 1.0°.
- Set the scattering slit to 1.0°.
- Set the receiving slit to 0.3mm.

- Now double-check your settings, and ensure they are correct. After verifying the settings are correct, now click the "OK" button.
- A window displays of "File and Sample Condition Edit" will pop-up. Now change the "Group Name" to make them match with the name of your sample. Also, change the "Sample Name" and "File Name", to ensure they are matching with the name of your sample. Now Click "New".

  You can create the samples later by changing the names of the sample and file, and clicking the "Modify" button.
- On the "Standard Condition Edit" window, click the "Close" button.

How to initiate the XRD processing.

- On the "XRD-6100/7000" panel, select the "Right Gonio Analysis" button.
- The name of your sample will appear in blue highlight on the upper section of the "Right Gonio System: Analysis Condition Edit Program" window. Select your sample and click the "Append "button. Your sample will be added on the list appearing at the bottom section of the "Entry for Analysis" window. After it's added, click the "Start" button. This action will make your sample

to appear at the bottom of the “Right Giono Analysis and Spooler Program” window. On the same window, click the “Start” button”. The analysis process will be started officially.

    - Analysis indicators: After the locking mechanism has locked on the sliding door, the XRD will produce a clicking sound. Also, a yellow light will be illuminated under “X-Rays On” icon, on XRD’s face.

- Open the software windows and let the XRD to analyze your sample for about approximately 30 minutes.

Indicators of a complete XRD Processing

- After the processing is complete, a whole peak spectrum will appear on the “Right Giono Analysis and Spooler Program” window.
- The green “Analyzing” box will disappear, while the yellow “X-Rays On” light will turn off.
- Follow the above process, if you need to analyze more samples.

How to Open the Peak Profile Spectrum

- On your desktop, click the “MDI jade 9” software icon.
- Click the “Read” button on the “file” section, and on the “favorites”, find the “xddat” folder and start searching for your samples folder.
- On your samples folder, every sample must feature a “Raw” file. You will be using the file to open the spectrum you have chosen in “Jade 9” software.

How to Identify Minerals in Peak Spectrum

Having a sufficient education background on the sample you intend to analyze is vital. You will highly lower the amount of time you will spend identifying the different peaks in the spectrum, if you have some knowledge about the bulk composition, and what you intend to determine.

- On the tool bar, move your cursor to the “Find Peaks”, which is located close to the “Floppy Disk” icon. You will use the icon in identifying and statically mark relevant peaks in the spectrum.
- Select a mineral database: Move your cursor at the top of the panel. A drop-down menu will open to the right of the spectrum window. On the menu, select the “RDB-Minerals” to be your database. You will predominately use the database in identifying most minerals that are within your spectra.
    - If there is no mineral in the selected database, switch to the “PDF +4 Minerals” database library. But, after locating the mineral, ensure you have switched back to the RDB database.
- Based on your knowledge about the analysis sample, start looking for minerals. Press the “Enter” button on your keyboard, after identifying minerals that suit your peak spectrum. The process adds the minerals in a compiled list of all the minerals you did identify on the spectrum.
- The “Line Based Match/Search” is an essential tool that you will utilize after you are done with your starting hypothetical list of minerals. Move your cursor to the primary tool bar and expand “Identify”. After expanding, choose the “Line Based Search” choice.
    - The tool will start compiling a list of minerals through searching a chose PDF database for entries that have peaks, and are statistical matches for all the peaks you have identified in your spectrum.
    - Settings:
        - The maximum setting for the [Two-Theta Error Window] should be equal to or less than 0.24%
        - The max setting for [Top Hits to List] should be 80.

- After setting the parameters, click the “Play” button, blue in color, which is next to the [X] button. This will search and create a list of phases that are likely to suit your spectra.

NB: You should not use the line-based search as your main way of identifying a bulk mode of the sample, because the software has no consistency in generating phases, and it is likely to omit vital phases of the spectrum.

Analysis of the model

- After all the minerals have been identified, press the “Enter” key on your keyboard, to check if all have been added in the list of minerals.
- To start the analysis of the model, move to the toolbar that is at the center of the window and click the [%] icon, which is placed next the drop-down mineral list.
    - An overlay with the results of the modal in form of various chart configurations will appear. Utilize the drop-down menu on the chart window to change the configurations.
- For the text format view of the modal analysis, click the […] icon, which is located near the [%] icon. The minerals will be listed by names, normal weight percent of every mineral and their chemical formula. Also, the format will state if the mineral component is a trace, minor, major or absent in your sample.
- To remove any mineral in your list of minerals whenever you want, select the mineral and press [Enter] on your keyboard. Use this method to remove absent phases.

Using Pattern Deconvolution for Analysis Check

- The use of a [Pattern Deconvolution] tool is a main indicator of whether your peak spectrum has been identified and fitted completely. The tool operates automatically with the modal analysis.
    - A red overlay spectrum will be produced on top of the original white spectrum by the tool.
    - The process will generate a [Best Fit Profile] which will be composed of the chosen mineral standards from the [Mineral PDF] database library and sample spectrum.
    - The red deconvolution overlay matches the peak spectra of every peak after proper identification of all the minerals. The presence of peaks without red deconvolution overlay indicates there was no identification of those peaks.
- Analysis of your spectrum should continue up to the point the original spectra matches the deconvolution spectra.

How to save your data

- On the files, click [Save]. However, ensure you have saved your data on "Current Work" as [*SAV]. The method saves all your analysis like a separate file.

Appendix B - GeoMark Research Geochemical Analysis Techniques and Procedures

Sample Requirement;

A minute amount (teaspoon) of sample material is necessary to do a TOC, vitrinite reflectance, residual hydrocarbon fluid fingerprinting and Rock-Eval. A tablespoon would be better, but a teaspoon would do just fine as well. It's entirely possible to get results from samples less than a teaspoon but this depends on the characteristics of the sample – amount of vitrinite and organic richness.

A sample must be prepped before undergoing testing such as being grinded using a mortar and pestle and gone through a 60-mesh sieve.

Use of LECO C230 Instrument to Get Total Organic Carbon

The rock sample, treated with hydrochloric acid, must go through decarbonation for it to be put through a LECO TOC analysis. The sample is placed in the concentrated hydrochloric acid for a minimum of two hours. The samples are rinsed off with water and put through a filtration device to get rid of the acid. Its then put in a LECO crucible and placed in an oven at a low temperature of 110 degrees Fahrenheit for four hours to dry out.

Once done, the samples are weighed based on the percentage of carbonate value.

The LECO C230 device is adjusted with standards using the known contents. The process is finalized by combusting them to a temperature of 1200 degrees Fahrenheit when oxygen is present. Both carbon dioxide and carbon monoxide are produced, with the carbon monoxide being changed into carbon dioxide using a catalyst.

An IR (infra-red cell) measures the carbon dioxide. A combustion of unknown test is done and the reaction of unknown per mass unit is equated to the calibration standard, which gives the TOC.

Standards are noted as being unknowns every 10 samples to determine the analysis' calibration and variation. Tests were carried out once more to determine data accuracy. A three percent variation was considered acceptable from the original value.

A Look at the Rock-Eval/HAWK Pyrolysis

The HAWK device reviewed about 100 mg of washed whole rock sample. These organic-rich samples were examined at a lesser weight when the S2 value surpasses 40mg/g or TOC goes beyond eight percent. These samples had to be reevaluated at the lower weight when the values were attained at 100mg.

RE-II Operating Environments

- S1 – 300 degrees Celsius for three minutes
- S2 – Between 300 and 550 degrees Celsius, increasing the temperature every 25 degrees per minute; then hold for another minute at 550 degrees Celsius
- S3 – Information attained at 300 to 390 degrees Celsius

RE-VI Operating Environments

- S1 – 300 degrees Celsius for three minutes
- S2 – Between 300 to 650 degrees Celsius, increasing the temperature every 25 degrees Celsius per minute and holding it at 650 degrees for a minute amount of time
- S3 – Measurements are taken between 300 and 400 degrees Celsius

HAWK Operating Environments

- S1 – 300 degrees for three minutes
- S2 – 300 to 650 degrees, increasing the temperature by 25 degrees each minute until it reaches 650 degrees Celsius, holding the temperature for a minute amount of time.
- S3 – Measurements are taken at temperatures between 300 and 400 degrees

Rock-Eval Measurements revealed the following:

- S1 – Free Oil Content
- S2 – Residual Generation Potential
- T_{max} – Temperature at the maximum S2 hydrocarbons evolution
- S3 – Yield of organic carbon dioxide

What were some of the useful ratios in the TOC data and Rock-Eval?

- Hydrogen Index – S2/TOC x 100
- Oxygen Index – S3/TOC x 100
- Normalized Oil Content – S1/TOC x 100
- Production Index – S1 (S1+S2)

With the use of a rock standard, device adjustments can be attained. These values are determined using an adjustment curve to pure hydrocarbons of various concentrations. The standard is reviewed after every 10 samples, noted being a device calibration. If the specifications are not met, the data attained is rejected. The devices are recalibrated, and the samples are reviewed once more.

The standard's normal variations are then adjusted to any variation. Under the guidelines below, the standard deviation is deemed acceptable.

T_{max} - +/- 2 degrees

S1 – 10 percent variation of proven value

S2 – 10 percent variation of proven value

S3 – 20 percent variation of proven value

The analytical information is checked at random in about 10 percent of the samples with a standard is reviewed as an unknown every 10 samples.

Turnaround Time:

The sample orders of the least year had a standard turnaround time of two to three weeks based on how many samples were sent.

References

Adams, J. E., 1965, Stratigraphic-tectonic development of Delaware Basin. AAPG Bulletin, v. 49, p. 2140–2148.

Alexander, J., Hall, D. H., Storey, B. C., 1981, Porosity measurements of crystalline rocks by laboratory and geophysical methods. Institute of Geological Sciences, Report EPNU, p. 81-10.

Barker, C. E., and Pawlewicz, M. J., 1987, The effects of igneous intrusions and higher heat flow on the thermal maturity of Leonardian and younger rocks, western Delaware basin, Texas, in D. W. Cromwell and L. Mazzulo, eds., Glass Mountain: SEPM Guidebook, p. 67–83.

Bereskin, S. R., Dube, G., Christiansen, Frantz, Jr., 2001, The Lewis Shale, San Juan Basin: Approaches to Rocky Mountain tight shale gas plays. Petroleum Technology Transfer Council Southwest Region Workshop: http://pttc.org/workshop _summaries/502.pdf.

Bertoncello, A., Wallace, J., Blyton, C., Honarpour, M., Kabir, C., 2014, Imbibition and water blockage in unconventional reservoirs: Well management implications during flow back and early production. Presented at the SPE/EAGE European Unconventional Resources Conference and Exhibition, Vienna, Austria; Paper No. SPE-167698-MS.

Bevers, J. R., 2017, Pore Structure characterization of reservoir and source rocks in the Bone Spring Formation, Lea County, New Mexico. AAPG Southwest Section, Article #90292.

Britt, L. K., Schoeffler, J., 2009, The geomechanics of a shale play: what makes a shale prospective. SPE125525, 9 pp.

Broadhead, R. F., Jianhua, Z., and Raatz, W. D., 2004, Play analysis of major oil reservoirs in the New Mexico part of the Permian Basin-Enhanced production through advanced technologies. Socorro, New Mexico Bureau of Geology and Mineral Resources, New Mexico Institute of Mining and Technology, Open-File Report 479, 134 p.

Bustin, R. M., 2006, Rethinking methodologies of characterizing gas in place in gas shales (abs.). AAPG Annual Meeting Program, v. 15, CD-ROM.

Cys, J. M., and Gibson, W. R., 1988, Pennsylvanian and Permian geology of the Permian Basin region, in Frenzel et al., 1988, The Permian Basin region, in L. L. Sloss, ed., Sedimentary cover—North American craton, U.S: Boulder, Colorado, Geological Society of America, The Geology of North America, v. D-2, p. 277–289.

DrillingInfo, 2018. www.drillinginfo.com

Encyclopedia Britannica, Inc., 02 May 2013. Web. 27 Mar. 2017. https://www.britannica.com/place/Permian-Basin

Energy Information Administration (EIA), 2014, Annual Energy Outlook 2014: With projections to 2040. https://www.eia.gov/outlooks/aeo/pdf/0383(2014).pdf

Energy Information Administration (EIA), 2018, Today in Energy: The United States exported more natural gas than it imported in 2017. https://www.eia.gov/todayinenergy/detail.php?id=35392

Energy Information Administration (EIA), 2018, Today in Energy: Permian region is expected to drive U.S. crude oil production growth through 2019. https://www.eia.gov/todayinenergy/detail.php?id=36936

Galley, J. E., 1958, Oil and Geology in the Permian Basin of Texas and New Mexico, in Weeks, L. G. editor, Habitat of Oil: American Association of Petroleum Geologists, Tulsa, OK., p. 395-446.

Gamero-Diaz, H., Miller, C.K., and Lewis, R., sCore: A mineralogy-based classification scheme for organic mudstones. SPE Annual Technical Conference and Exhibition, Presentation at the Society of Petroleum Engineers, New Orleans, LA, USA, September 30, 2013, 10.2118/166284-MS.

Gao, Z., and Hu, Q., 2013, Estimating permeability using median pore-throat radius obtained from mercury intrusion porosimetry. Journal of Geophysics and Engineering, v. 10, p. 025014.

Hager, J., 1998. Steam Drying of Porous Media. Ph.D. Thesis, Department of Chemical Engineering, Lund University, Sweden, 155 pp.

Handford, C.R., 1981, Sedimentology and genetic stratigraphy of Dean and Spraberry formations (Permian), Midland Basin, Texas. AAPG Bulletin, v. 65, no.9, p.1602-1616.

Harris, N. B., Miskimins, J. L., Mnich, C. A., 2011, Mechanical anisotropy in the Woodford shale, Permian Basin: Origin, magnitude, and scale. Leading Edge, v. 30, no. 3, p. 284–291,

Hills, J. M., 1984, Sedimentation, tectonism, and hydrocarbon generation in Delaware Basin, west Texas and southeastern New Mexico. AAPG Bulletin, v. 68, p. 250-267.

Hills, J. M., 1985, Structural evolution of the Permian Basin of west Texas and New Mexico, in P. W. Dickerson and W. R. Muehlberger, eds., Structure and tectonics of trans-Pecos Texas, West Texas Geological Society Guidebook, Midland, Texas, v. 85–81, p. 89–99.

Hills, J. M., and Galley, J. E.., 1988, General introduction, the pre-Pennsylvanian Tobosa Basin, in Frenzel et al., 1988, The Permian Basin region, in L. L. Sloss, ed., Sedimentary cover—North American craton, U.S: Boulder, Colorado, Geological Society of America, The Geology of North America, v. D-2, p. 261–277.

Howard, J. J., 1991, Porosimetry measurement of shale fabric and its relationship to illite/smectite diagenesis. Clays and Clay Minerals, 39 (4), pp. 355-361

Hu, Q. H., Zhang, Y. X., Meng, X. H., Li, Z., Xie, Z. H., Li, M. W., 2017. Characterization of multiple micro-nano pore networks in shale oil reservoirs of Paleogene Shahejie Formationin Dongying Sag of Bohai Bay Basin, East China. Petroleum Exploration and Development, 44(5): 720–730.

Hu, Q., Ewing, R. P., Rowe, H. D., 2015, Low nanopore connectivity limits gas production in Barnett formation. Journal of Geophysical Research: Solid Earth 120 (12), 8073-8087

Hughes, J.D., 2014, Drilling Deeper: A Reality Check on U.S. Government Forecasts for a Lasting Tight Oil and Shale Gas Boom. Post Carbon Institute.

IHS Markit, 2018, Fixing the Permian mismatch: Upstream growth and mid-stream takeaway capacity. https://ihsmarkit.com/research-analysis/fixing-permian-mismatch-upstream-growth-midstream-take-away-capacity.html

Ingram, G. M., Urai, J. L., 1999, Top seal leakage through faults and fractures: The role of mudrock properties, in A. C. Aplin, A. J. Fleet, and J. H. S. Macquaker, eds., Muds and mudstones: Physical and fluid flow properties: Geological Society (London) Special Publication 158, p. 125–136.

Jarvie, D. M., 2008, Geochemical Characteristics of the Devonian Woodford Shale. Presented at Oklahoma Gas Shales meeting 22 October 2008, Oklahoma City, Oklahoma.

Kinley, T. J., Cook, L. W., Breyer, J. A., Jarvie, D. M., Busbey, A. B., 2008, Hydrocarbon potential of the Barnett Shale Mississippian, Delaware Basin, West Texas and Southeastern New Mexico. AAPG Bulletin, v. 92, no. 8, p. 967–991.

Kuila, U., McCarty, D. K., Derkowski, A., Fischer, T. B., Prasad, M., 2014, Total porosity measurement in gas shales by the water immersion porosimetry (WIP) method: Fuel, 117, 1115–1129, doi: https://doi.org/10.1016/j.fuel.2013.09.073. [PubMed]0016-2361

Ma, S., Zhang, X., Morrow, N., Zhou, X., 1999, Characterization of wettability from spontaneous imbibition measurements. Journal of Canadian Petroleum Technology, 38 (13), PETSOC-99-13-49.

McDade, E. C., Sassen, R., Wenger, L. M., Cole, G. A., 1993, Identification of Organic-rich Lower Tertiary shales as petroleum source rocks, south Louisiana: Gulf Coast Association of Geological Societies Transactions, v. 43, p. 257–267.

Montgomery S. L., 1997, Permian Bone Spring formation: sandstone play in the Delaware basin, part II-basin. AAPG Bulletin, v. 81, p. 1423-1434.

National Research Council, 1996, Rock Fractures and Fluid Flow: Contemporary Understanding and Applications. Washington, DC, The National Academies Press. https://doi.org/10.17226/2309.

Nester, P., Schwartz, K., Bishop, J., Garcia-Barriuso, M., and Chevron Corporation, 2014, The Avalon Shale: Tying Geologic Variability to Productivity in a Burgeoning Shale Play in the Delaware Basin of Southeast New Mexico. URTeC, DOI 10.15530/urtec-2014-1922929

New Mexico Energy, Minerals and Natural Resources Department, 2012, EMNRD Oil Conservation Division: NM OCD Oil and Gas Map. http://nm-emnrd.maps.arcgis.com/apps/webappviewer/index.html?id=4d017f2306164de29fd2fb9f8f35ca75

Roychaudhuri, B., Tsotsis, T., Jessen, K., 2011, An experimental and numerical investigation of spontaneous imbibition in gas shales. Presented at the 2011 SPE Annual Technical Conference and Exhibition, Denver, CO, USA; Paper No. SPE 147652

Sarg, J. F., Markello, J. R., and Weber, L. J., 1999, the second-order cycle, carbonate-platform growth, and reservoir, source, and trap prediction. P.M Harris, A.H Saller, J.A Simo (Eds.), Advances in Carbonate Sequence Stratigraphy: Application to Reservoirs, Outcrops and Models, Society of Economic Paleontologists and Mineralogists Special Publication, 63 (1999), pp. 11-34

Shakir, M. S., Anwar-ul-Hassan, Razzaq, A., 2002, Effects of salts on bulk density, particle density and porosity of different soil series. Asian Journal of Plant Sciences, 1:5-6, DOI: 10.3923/ajps.2002.5.6.

Shepard, T. M., Walper, J. L., 1982, Tectonic evolution of Trans-Pecos Texas. Transactions Annual Meeting, Gulf Coast Section, Geological Society of America, 32, 74-83.

Washburn, E. W., Bunting, E. N., 1922, Porosity: V. Recommended procedures for determining porosity by methods of absorption. Journal of American Ceramic Society, 5 (1), pp. 48-56

Washburn, E.W., 1921, Note on a Method of Determining the Distribution of Pore Sizes in a Porous Material. Proceedings of the National Academy of Sciences of the United States of America, v. 7, p. 115-116.

Worrall, J., and Krankawsky, C., 2011, Geology and development of the Bone Spring Formation in Loving County and adjacent areas: Part II Avalon Shale. AAPG Search and Discovery Article #90129, Southwest Section Meeting.

Yang, R., Guo, X., Yi, J., Fang, Z., Hu, Q., He, S., 2017, Spontaneous imbibition of three leading shale formations in the Middle Yangtze Platform, South China. Energy & Fuels, 31 (7), pp. 6903-6916.